

bradscholars

The RAC1 target NCKAP1 plays a crucial role in progression of BRAF/PTEN -driven melanoma in mice

Item Type	Article
Authors	Swaminathan, Karthic;Campbell, A.;Papalazarou, V.;Jaber-Hijazi, F.;Nixon, C.;McGhee, E.;Strathdee, D.;Sansom, O.J.;Machesky, L.M.
Citation	Swaminathan K, Campbell A, Papalazarou V et al (2021) The RAC1 target NCKAP1 plays a crucial role in progression of BRAF/PTEN -driven melanoma in mice. Journal of Investigative Dermatology. 141(3): 628-637.
DOI	https://doi.org/10.1016/j.jid.2020.06.029
Rights	© 2021 Elsevier. Reproduced in accordance with the publisher's self-archiving policy. This manuscript version is made available under the CC-BY-NC-ND 4.0 license (https://creativecommons.org/licenses/by/4.0/)
Download date	2025-05-20 03:28:24
Link to Item	http://hdl.handle.net/10454/18032

Journal Pre-proof

The RAC1 target NCKAP1 plays a crucial role in progression of BRAF/PTEN -driven melanoma in mice

Karthic Swaminathan, Andrew Campbell, Vassilis Papalazarou, Farah Jaber-Hijazi, Colin Nixon, Ewan McGhee, Douglas Strathdee, Owen J. Sansom, Laura M. Machesky

PII: S0022-202X(20)31956-4

DOI: <https://doi.org/10.1016/j.jid.2020.06.029>

Reference: JID 2574

To appear in: *The Journal of Investigative Dermatology*

Received Date: 5 March 2020

Revised Date: 24 June 2020

Accepted Date: 29 June 2020

Please cite this article as: Swaminathan K, Campbell A, Papalazarou V, Jaber-Hijazi F, Nixon C, McGhee E, Strathdee D, Sansom OJ, Machesky LM, The RAC1 target NCKAP1 plays a crucial role in progression of BRAF/PTEN -driven melanoma in mice, *The Journal of Investigative Dermatology* (2020), doi: <https://doi.org/10.1016/j.jid.2020.06.029>.

This is a PDF file of an article that has undergone enhancements after acceptance, such as the addition of a cover page and metadata, and formatting for readability, but it is not yet the definitive version of record. This version will undergo additional copyediting, typesetting and review before it is published in its final form, but we are providing this version to give early visibility of the article. Please note that, during the production process, errors may be discovered which could affect the content, and all legal disclaimers that apply to the journal pertain.

© 2020 The Authors. Published by Elsevier, Inc. on behalf of the Society for Investigative Dermatology.



The RAC1 target NCKAP1 plays a crucial role in progression of BRAF/PTEN -driven melanoma in mice

Karthic Swaminathan ^{1,2}, Andrew Campbell ¹, Vassilis Papalazarou ^{1,3}, Farah Jaber-Hijazi ^{1,4},
Colin Nixon ¹, Ewan McGhee ¹, Douglas Strathdee ¹, Owen J. Sansom ^{1,5}, Laura M.
Machesky ^{1,5*}

1. CRUK Beatson Institute for Cancer Research, Garscube Estate, Switchback Road,
Bearsden, Glasgow, G61 1BD, UK

2. Current address: Centre for Skin Sciences, Faculty of Life Sciences, University of
Bradford, Bradford, BD7 1DP, UK

3. School of Engineering, University of Glasgow, James Watt South Building, G12 8QQ

4. Current Address: School of Health and Life Sciences, University of the West of Scotland,
Paisley, PA1 2BE, UK

5. Institute of Cancer Sciences, University of Glasgow, Garscube Campus, Switchback Road,
G61 1QH, UK

*Author for correspondence L.Machesky@beatson.gla.ac.uk

Abstract

BRAF^{V600E} is the most common driver mutation in human cutaneous melanoma and is frequently accompanied by loss of the tumor suppressing phosphatase PTEN. Recent evidence suggests a co-operative role for RAC1 activity in BRAF^{V600E}-driven melanoma progression and drug resistance. However, the underlying molecular mechanisms and the role of RAC1 downstream targets are not well explored. Here, we examine the role of the NCKAP1 subunit of the pentameric cytoskeletal SCAR/WAVE complex, a major downstream target of RAC1, in a mouse model of melanoma driven by BRAF^{V600E}; PTEN loss. The SCAR/WAVE complex is the major driver of lamellipodia formation and cell migration downstream of RAC1 and depends on NCKAP1 for its integrity. Targeted deletion of *Nckap1* in the melanocyte lineage delayed tumor onset and progression of a mutant *Braf*; *Pten* loss driven melanoma mouse model. *Nckap1* depleted tumors displayed fibrotic stroma with increased collagen deposition concomitant with enhanced immune infiltration. *Nckap1* loss slowed proliferation and tumor growth, highlighting a role in cell cycle progression. Altogether, we propose that NCKAP1-orchestrated actin polymerization is essential for tumor progression and maintenance of tumor tissue integrity in a mutant *Braf*; *Pten* loss driven mouse model for melanoma.

INTRODUCTION

Metastatic cutaneous melanoma remains a major health problem, even though insights into the genetic drivers have increased therapeutic options (Merlino et al., 2016). BRAF is a serine/threonine kinase acting mainly through the MAPK pathway. Activating mutations in the *BRAF* gene, including BRAF^{V600E}, are major drivers of cutaneous melanoma and targeted therapies, such as vemurafenib, have allowed suppression of oncogenic signalling, improving therapeutic outcomes. In addition, immunotherapies, such as anti-PD1 or anti-CTLA-4 monoclonal antibodies can reprogramme the immune system against tumors. These advancements have in some cases have resulted in major survival improvements for metastatic melanoma (reviewed in Gellrich et al., 2020). However, tumor heterogeneity and emergence of resistance during treatment imposes a need for better understanding the underlying mechanisms of cutaneous melanoma progression (Gellrich et al., 2020). Preclinical mouse models mimic common human oncogene/tumor suppressor combinations and recapitulate disease progression (Perez-Guijarro et al., 2017). In mice, expression of BRAF^{V600E} from the endogenous locus, in the melanocytic lineage using Tyrosinase promoter driven Cre (Tyr::Cre), drives naevi formation and dermal expansion of melanocytes (Dhomen et al., 2009). Combination with deletion of the tumor suppressor *Pten*, a genetic event that co-occurs with BRAF^{V600E} in a significant proportion of human melanomas, led to aggressive disease in mice (Dankort et al., 2009).

RAC1 mutations occur in 8-10% of sun-exposed melanomas, most commonly a proline to serine P29S mutation (Halaban, 2015). *RAC1* encodes for a small GTPase which is a major regulator of actin cytoskeleton dynamics and RAC1^{P29S} is a more active variant (reviewed in (Li and Machesky, 2013). *RAC1*^{P29S} may also drive resistance to BRAF inhibition and alter

cell surface expression of PD1 (Watson et al., 2014). *RAC1*^{P29S} expression in a mouse model can drive transcriptional reprogramming *via* the actin-responsive serum response factor SRF or the RAC1-binding kinase PAK (Lionarons et al., 2019). However, the involvement of the SCAR/WAVE complex, a major cytoskeletal effector of RAC1 activity, has not been explored in melanoma. The SCAR/WAVE complex consists of five subunits: NCKAP1, CYFIP1, ABI1, SCAR/WAVE, HSPC300 and their isoforms (Pollitt and Insall, 2009). The different subunits function together, with CYFIP1 and NCKAP1 being core subunits (Ibarra et al., 2006, Steffen et al., 2004, Tang et al., 2013). The SCAR/WAVE complex drives remodelling of the actin cytoskeleton in response to activation of RAC1, promoting cell migration and uptake of nutrients from the microenvironment *via* macropinocytosis or phagocytosis (Stradal et al., 2004) (Steffen et al., 2004).

Regardless of the *RAC1* mutational status, loss of PTEN enhances PI-3-kinase signaling, leading to a positive feedback loop for activation of RAC1 (Chalhoub and Baker, 2009). The SCAR/WAVE complex is a well-established direct target of RAC1 activation (Chen et al., 2017). We deleted the gene coding for the NCKAP1 subunit in BRAF^{V600E}/PTEN loss-driven melanomas in mice and found that loss of *Nckap1* significantly reduced tumor burden and slowed tumour growth. *NCKAP1* deletion led to altered signalling, increased tumor fibrosis and enhanced infiltration by several immune cell types. Taken together, our data suggest an important role of the SCAR/WAVE complex in melanoma progression driven by BRAF^{V600E} mutation and PTEN loss.

RESULTS

Loss of the RAC1 target NCKAP1 delayed the onset and development of melanoma.

RAC1 plays an essential role in *Tyr::Nras^{Q61K}* driven melanoma and melanocytic dermal expansion (Li et al., 2012). However, the role of RAC1 downstream effectors such as the SCAR/WAVE complex are largely unknown. Therefore, we generated a mouse model with conditional deletion of *Nckap1* (**Figure S1a**, Methods). We crossed *Nckap1^{ff}* conditional mice with an established malignant melanoma mouse model, *Tyr::CreER^{T2+};Braf^{V600E+};Pten^{wt/f}* (Dankort et al., 2009, Dhomen et al., 2009, Suzuki et al., 2001), to assess the role of NCKAP1 in melanoma progression (**Figure S1b**).

Mice carrying the genotype *Tyr::CreER^{T2+};Braf^{V600E+};Pten^{wt/f};Nckap1^{wt/wt}* and *Tyr::CreER^{T2+};Braf^{V600E+};Pten^{wt/f};Nckap1^{ff}*, hereafter referred as *Nckap1^{wt/wt}* and *Nckap1^{ff}* mice, were induced by skin painting (Methods and Table S1), leading to *Braf^{V600E}* expression together with loss of *Pten* (heterozygous) and *Nckap1* (homozygous) alleles in the melanocytic lineage (**Figure S1b-d**). *Nckap1^{wt/wt}* mice developed primary melanoma with expected penetrance and latency to previous observations (Dankort et al., 2009) and therefore were used as littermate controls. Both *Nckap1^{ff}* and *Nckap1^{wt/wt}* mice developed naevi (e.g. clusters of pigmented dermal melanocytes) and tumors (e.g. larger clusters both pigmented and unpigmented and penetrated deeper into the dermis) (**Figure 1a-b**), which were allowed to grow until the largest reached 1.2 cm in diameter. The number of tumors in *Nckap1^{ff}* mice (average 1.71±0.25 tumors/mouse: n=16 mice; p<0.0001) was reduced compared to *Nckap1^{wt/wt}* mice (average 6.75±0.9 tumors/mouse: n=14 mice) (**Figure 1c**). Tumor burden at endpoint was also reduced in *Nckap1^{ff}* (n=16 mice; 662.6±84.4 mm³; p<0.01) compared to *Nckap1^{wt/wt}* mice (n=14 mice; 1260±133 mm³) (**Figure 1d**). Tumors from *Nckap1^{wt/wt}* and *Nckap1^{ff}* mice displayed similar morphology (**Figure 1e-f**). Thus, *Nckap1* is important for initiation of melanoma tumours and tumour growth in this model.

Loss of *Nckap1* delayed tumor growth

Since the tumours showed delayed growth in the absence of NCKAP1, we examined the tumour growth kinetics. *Nckap1^{ff}* tumors (mean±SEM; 2.34±0.7, n=5 mice) showed a significantly ($P<0.05$) lower percentage of BrdU positive nuclei per mm² compared to *Nckap1^{wt/wt}* tumors (mean±SEM; 5.18±0.7, n=5 mice) (**Figure 2a-b**). This was not likely due to a failure to enter the cell cycle, as the %Ki67 positive nuclei per mm² in *Nckap1^{ff}* (mean±SEM; 25.18±1.78; n=7 mice) was similar to *Nckap1^{wt/wt}* (mean±SEM; 26.71±2.74, n=5 mice) tumors (**Figure 2c-d**). However, there was a significant reduction ($P < 0.01$) in cyclin D1 positive nuclei/mm² in *Nckap1^{ff}* (mean±SEM; 15.02 ±3.23, n=8 mice) compared with *Nckap1^{wt/wt}* (mean±SEM; 38.95 ± 6.00, n=8 mice) (**Figure 2e-f**), indicating a delay in G1 cell cycle progression. The average size of *Nckap1^{wt/wt}* and *Nckap1^{ff}* tumors from the day of first appearance was also reduced in *Nckap1^{ff}* (**Figure 2g and Table S2**). Tumors from *Nckap1^{ff}* (n=7 mice) expanded more slowly compared to *Nckap1^{wt/wt}* (n=7 mice). Average tumor size in *Nckap1^{ff}* mice was 46.75 ± 9.18 mm³ which is significantly smaller than the average tumor size of 164.1 ± 15.04 mm³ ($P < 0.0001$) in *Nckap1^{wt/wt}* at **day 14**; 62.07 ± 18.11 mm³ in *Nckap1^{ff}* and 326.6 ± 45.55 mm³ ($P < 0.001$) in *Nckap1^{wt/wt}* at **day 21**; 146.1 ± 30.08 mm³ in *Nckap1^{ff}* and 569.5 ± 70.32 mm³ ($P < 0.0001$) in *Nckap1^{wt/wt}* at **day 28**. Thus, loss of *Nckap1* slowed cancer cell cycle progression and proliferation of melanomas, leading to fewer and smaller lesions at comparable time points. This phenotype is reminiscent of the role of RAC1 downstream of NRAS in *NRas^{Q61K}* and loss of *Ink4a^{-/-}* mouse melanoma model (Ackermann et al., 2005 and Li et al., 2012a), suggesting that the SCAR/WAVE complex may be important for cell cycle progression downstream of RAC1 in melanoma.

Loss of *Nckap1* delayed melanocyte dermal expansion, nevus appearance and tumor onset

We next explored the various stages of melanoma progression and noticed a significant ($P < 0.01$) delay in the appearance of nevi in the back skin after tamoxifen induction in *Nckap1^{ff}* (Mean±SEM; 61.21±3.12 days; n=14 mice) compared to *Nckap1^{wt/wt}* mice (Mean±SEM; 43.87±2.75 days; n=15 mice) (**Figure 3a**). *Nckap1^{ff}* mice also showed delayed progression from naevus to tumor (Mean±SEM; 8.66±1.58; n=11 mice) compared to *Nckap1^{wt/wt}* (Mean±SEM; 32.67±6.85; n=15 mice) and tumor-free survival was extended by ~150% in *Nckap1^{ff}* compared to *Nckap1^{wt/wt}* (median tumor-free survival from 52 to 78 days) (**Figure 3b and Figure S1e**). It was previously observed that constitutive expression of mutant NRas^{Q61K} in the melanocyte lineage led to RAC1-dependent postnatal dermal expansion of melanocytes (Li et al., 2012). Given that RAC1 activates Nckap1, we quantified dermal melanocyte clusters from *Nckap1^{wt/wt}* and *Nckap1^{ff}* back skin in endpoint 1.2cm tumours (**Fig 3c-d**). The percentage of pigmented area (melanocyte clusters)/mm² was 14.59±2.07 (mean±SEM) for *Nckap1^{ff}* (n=6 mice) which was significantly higher ($P < 0.05$) than 8.23±1.59 (mean±SEM) for *Nckap1^{wt/wt}* (n=8 mice) (**Figure 3e**), indicating that dermal expansion of melanocytes still occurs in Nckap1 knockouts, but that de-differentiation as demonstrated by Laurette (Laurette et al., 2020) may be affected by loss of Nckap1. The number of pERK (p42/44, extracellular related signal kinase) positive cells/mm² was similar ($P = 0.38$) between *Nckap1^{ff}* (mean±SEM; 8.00±1.85; n=6 mice) and *Nckap1^{wt/wt}* tumors (mean±SEM; 11.88±4.02; n=5 mice) (**Figure S2a-c**) suggesting NCKAP1 is dispensable for ERK signaling downstream of BRAf^{V600E}. Due to the delay in tumor appearance and slow growth of tumors, the median survival time (endpoint = largest tumor is 1.2cm) of *Tyr::CreER^{T2+};Braf^{V600E+};Pten^{wt/f}* mice was extended by ~160.9% (median survival from

84.5 to 136 days) upon *Nckap1* loss (**Figure 3f**) with ($P < 0.0001$) by Log-rank (Mantel-cox) test. Altogether, *Nckap1* is dispensable for dermal expansion, but plays an important role in naevus formation and progression to melanoma tumors.

***Nckap1* loss induces fibrosis in *Braf*^{V600E} *PTEN* loss-driven melanoma.**

Extracellular matrix (ECM) drives tumor progression and metastasis (Hynes, 2009, Lu et al., 2012, Naba et al., 2016). Collagen is one of the major ECM proteins aiding tumor survival and growth (Lu et al., 2012) and high levels of collagens correlate with poor outcome in human melanomas (Miskolczi et al., 2018). Picrosirius red staining of tumours of identical endpoint size range showed a strong deposition of collagen in *Nckap1*^{ff/ff} compared to *Nckap1*^{wt/wt} tumors (**Figure 4a, b**). Specifically, the percentage of picrosirius red positive areas/mm² was significantly ($P < 0.05$) increased in *Nckap1*^{ff/ff} tumors (mean±SEM; 57.66±9.08; n=6 mice) compared to *Nckap1*^{wt/wt} tumors (mean±SEM; 32.87±5.64; n=7 mice) (**Figure 4c and Figure S3a-d**). Two-photon microscopy and second harmonic imaging of freshly prepared tumor sections (Rath et al., 2017) revealed the organisation (correlation) of the collagen to be similar (**Figure 4d**), however, *Nckap1*^{ff/ff} tumors (n=11) contained substantially more collagen (homogeneity) than *Nckap1*^{wt/wt} tumors (n=11) (**Figure 4e**). TGFβ signaling is important for ECM deposition and we observed that nuclear pSMAD3 (downstream TGFβ target) was significantly ($p < 0.05$) elevated in *Nckap1*^{ff/ff} (n = 6) compared to control *Nckap1*^{wt/wt} tumors (n = 5) potentially implicating TGFβ signalling in the fibrotic response (**Figure S3e-g**). Cancer associated fibroblasts (CAFs) are a major source of collagen in the tumour microenvironment (Franco et al., 2010), but the total α-SMA (alpha smooth muscle actin, CAF marker) positive area was similar between *Nckap1*^{wt/wt} and *Nckap1*^{ff/ff} tumors (mean±SEM; 39.35±6.285 in *Nckap1*^{wt/wt} n=8 mice; 42.28±6.04 in *Nckap1*^{ff/ff} n=8 mice) (**Figure 4f**).

Constitutive BRAF^{V600E} expression induces senescence through accumulation of p21, p16^{INK4A}, and p53 cell cycle blockers (Dhomen et al., 2009). Therefore, we queried whether *Nckap1* loss could affect tumor senescence by quantifying p21 positive cells from *Nckap1*^{wt/wt} and *Nckap1*^{ff} tumors (**Figure S4a-b**) but found no difference between *Nckap1*^{ff} tumors (mean±SEM; 42.70±5.14; n=8 mice) and *Nckap1*^{wt/wt} tumors (mean±SEM; 49.71±2.14; n=11 mice) (**Figure S4a-c**). So, while loss of *Nckap1* enhances fibrosis, it does not drive excessive recruitment of α -SMA positive CAFs or obvious senescence.

NCKAP1 engages ECM and links nutrient signals in *Braf*^{V600E} PTEN loss-driven melanoma.

We asked if the excessive fibrotic matrix in *Nckap1*^{ff} tumors might drive YAP transcriptional activation. Indeed, the percentage of YAP positive cells/mm² was significantly increased ($P<0.05$) in *Nckap1*^{ff} tumors (mean±SEM; 20.18±3.66 ; n=6 mice) compared to *Nckap1*^{wt/wt} tumors (mean±SEM; 7.54±1.62; n=6 mice) (**Figure S5a-c**). While the adhesion and oncogenic kinase Src was a candidate driver, the number of active Src (pSrc-Tyr416) positive cells/mm² was significantly ($P<0.01$) lower in *Nckap1*^{ff} tumors (mean±SEM; 68.77±10.57, n=7 mice) compared to *Nckap1*^{wt/wt} tumors (mean±SEM; 128.4±15.41, n=7 mice) (**Figure S5d-f**). Thus, although nuclear YAP in melanomas can be driven by fibrosis associated with loss of *Nckap1*, this is not accompanied by increased phospho-Src and surprisingly is independent of actin dynamics downstream of the SCAR/WAVE complex.

Mammalian Target of Rapamycin (mTOR) links nutrient availability to tumor growth and its activity depends on SCAR/WAVE complex-mediated signaling (Rainero et al., 2015). We therefore measured the activation status of mTOR using anti-phospho-S6 (Ribosomal Protein – Ser235/236), a well-known mTOR activity reporter. The percentage of pS6 positive cells/mm² was significantly ($P<0.05$) lower in *Nckap1*^{ff} tumors (mean±SEM; 24.30±5.31;

n=8 mice) compared to *Nckap1*^{wt/wt} tumors (mean±SEM; 46.90±6.08; n=8 mice) (**Figure S6a-c**) indicating a link between NCKAP1 and nutrient sensing and growth in tumours.

***Nckap1* loss induces HIF1 α expression and reduced vascularization in mutant *Braf* ;
Pten loss-driven melanoma.**

Expression of hypoxia-inducible transcription factor (HIF1 α) correlates with fibrosis and collagen deposition in cancers (Gilkes et al., 2014). We thus stained serial sections of *Nckap1*^{wt/wt} and *Nckap1*^{ff} tumors for S100 (melanoma marker), HIF1 α and CD31 (vasculature) (**Figure 5a-h**). HIF1 α expression was highly enriched in the stromal cells surrounding S100 positive areas in *Nckap1*^{ff} tumors compared to *Nckap1*^{wt/wt} tumors (**Figure 5a,b,d,e**). The percentage of HIF1 α positive area/mm² was significantly ($P<0.01$) higher in *Nckap1*^{ff} tumors (mean±SEM; 41.67±5.58; n=7 mice) compared to *Nckap1*^{wt/wt} tumors (mean±SEM; 16.82±4.89; n=7 mice) (**Figure 5g**). In addition, the percentage of CD31 positive area/mm² was significantly ($P<0.001$) lower in *Nckap1*^{ff} tumors (mean±SEM; 1.54±0.15; n=9 mice) compared to *Nckap1*^{wt/wt} tumors (mean±SEM; 2.59±0.19; n=9 mice) (**Figure 5h**). TUNEL staining for cell death revealed no significant change in positive nuclei/mm² in *Nckap1*^{ff} tumors (mean±SEM; 41.15±10.08; n=5 mice) vs 49.95±11.67 in *Nckap1*^{wt/wt} tumors (mean±SEM; 49.95±11.67; n=5 mice) (**Figure 5i-k**). Thus NCKAP1 may have a role in regulation of hypoxia due to stromal accumulation and reduced vascularity, thereby regulating melanoma growth.

***Nckap1* loss induces increased immune infiltration in mutant *Braf* ; *Pten* loss driven melanoma.**

We next asked whether increased collagen deposition and hypoxic signature were associated with an inflammatory response. The total number of CD8+ cells/mm² was significantly ($P<0.05$) increased in *Nckap1^{ff/ff}* tumors (mean±SEM; 328.8±33.11; n=7 mice) compared to *Nckap1^{wt/wt}* tumors (mean±SEM; 174.9±39.73; n=7) (**Figure 6a-c**). Moreover, *Nckap1^{ff/ff}* tumors showed a significantly ($P<0.01$) increased number of CD4+ T-cells/mm² (mean±SEM; 20.27±3.50, n=7 mice) than *Nckap1^{wt/wt}* tumors (mean±SEM; 6.95±2.02; n=7 mice) (**Figure S7a-c**). The increased T-cell infiltration also correlated with significantly ($P<0.01$) increased CD3+ cell staining in *Nckap1^{ff/ff}* tumors (mean±SEM; 24.79±4.28 from n=7 *Nckap1^{ff/ff}* tumors; 9.71±1.76 from n=7 *Nckap1^{wt/wt}* tumors) (**Figure S7d-f**). Next, we investigated the presence of mast cells using toluidine staining. The total number of mast cells/mm² was significantly ($P<0.01$) higher in *Nckap1^{ff/ff}* tumors (mean±SEM; 26.73±3.31, n=7 mice) compared to *Nckap1^{wt/wt}* tumors (mean ±SEM; 11.07±1.90, n=7 mice) (**Figure 6d-f**). There was no significant difference in the total number of F4/80 positive (macrophage) cells/mm² in *Nckap1^{ff/ff}* (mean±SEM; 2574±289.7, n=6 mice) compared to *Nckap1^{wt/wt}* tumors (mean±SEM; 2192±450.3; n=6 mice) (**Figure 6g-i**). We further asked if this increased infiltration of immune cells is a result of enhanced cytokine production in the tumors using a mouse cytokine array (111 cytokines, Proteome Profiler Mouse XL Cytokine panel, see Methods and **Figure S8a-b, Table S3**). There was no major difference between *Nckap1^{wt/wt}* and *Nckap1^{ff/ff}* tumors regarding the production of interleukins 2-15 or other pro-inflammatory signal mediators detected. A few of the more significant changes are highlighted in **Figure S8c**. Altogether, our data suggest that genetic loss of *Nckap1* enhances infiltration of anti-tumor immune cells, which may serve to restrain tumour growth.

DISCUSSION

The small GTPase RAC1 is an important driver of cutaneous melanoma (Halaban, 2015) but is not yet druggable. RAC1 drives dermal melanocyte survival and tumor progression and metastasis in an *NRas*^{Q61K} driven genetic model (Li et al., 2012). RAC1 is a major upstream regulator of NCKAP1; a member of the SCAR/WAVE complex and is frequently mutated to an activated state (P29S mutation) or overexpressed in human melanomas (Li and Machesky, 2013). We thus explored the potential role of the WAVE complex subunit NCKAP1, in BRAF^{V600E}/PTEN loss driven melanoma. While NCKAP1 is not apparently amplified or altered in melanomas (e.g. cBioportal TCGA data), it is a crucial effector of Rac1 mediating actin dynamics and is likely activated by oncogenic signalling in melanomas. Here we show that deletion of NCKAP1 in a mouse model of BRAF PTEN loss driven melanoma delayed nevus formation and tumor progression significantly.

RAC1 drives cell cycle progression in melanoma and other cancers (Molinie et al., 2019). We previously identified a role of RAC1 (*in vivo*) and the WAVE complex (in cell culture) in the migration of melanoblasts (Li et al., 2012), but little is known about a possible role for WAVE complex or the subunit NCKAP1 in cell cycle progression in cancer. Here, we implicate NCKAP1 in onset of naevus and melanoma development and cyclin D1 expression leading to cell cycle progression. Nuclear pSMAD3 increased in Nckap1 knockout tumours, indicating a possible involvement of TGF- β signaling. NCKAP1 may thus propagate Rac1 signaling in a positive feedback loop driving cell cycle progression. RAC1 signaling depends on PI3K, which is known to drive nuclear cyclin D1 and cell cycle progression (Bailey et al., 2017, Lionarons et al., 2019). Branched actin downstream of WAVE complex is essential for cell cycle progression, further supporting the idea that positive feedback between RAC1 and its downstream targets could contribute to tumor progression (Molinie et al., 2019). Another factor in driving cell cycle progression might be *via* mTOR, which is important for tumor

growth in the *Braf Pten* mouse melanoma model (Damsky et al., 2015). Phosphorylation of ribosomal S6 protein was reduced in *Nckap1^{fl/fl}* in agreement with the previously reported role for NCKAP1 in nutrient sensing via integrin and ECM endocytosis (Rainero et al., 2015). Thus, NCKAP1 likely promotes melanoma tumor growth through adhesion-mediated cyclinD1 expression and nutrient sensing.

Loss of *Nckap1* in mutant *Braf;Pten^{fl/wt}* tumors induced a highly fibrotic phenotype and enhanced nuclear Yap, consistent with increased pSMAD3 in *Nckap1* knockout tumours. Fibrosis is observed in the rare desmoplastic type of melanoma (DeWane et al., 2019) and also in other cutaneous melanoma types during acquisition of resistance to BRAF inhibitors and is associated with activation of the Yap/Taz and MRTF transcriptional pathways (Girard et al., 2020). BRAF-resistant melanomas can develop a “drug-protective” stroma (Girard et al., 2020) that activates Yap-dependent growth pathways and protects tumour cells from exposure to inhibitors. YAP can drive tumour differentiation downstream of TGF- β signaling in melanomas (Miskolczi et al., 2018). In the presence of increased stromal collagen and high TGF- β , SMAD and YAP-TEAD complexes led to dedifferentiated slow cycling tumors, while in the absence of TGF- β YAP-PAX3 signaling drive MITF high differentiated and proliferative tumors (Miskolczi et al., 2018). NCKAP1 knockout tumours also displayed hallmarks of differentiation such as increased melanin staining (e.g. see Figure 1e, f), but they were not proliferative. The mechanism of collagen accumulation in NCKAP1 tumors is not clear, but could involve a role of NCKAP1 in MMP secretion (e.g. Figure S8c) or a feedback loop related to enhanced immune cell recruitment.

Nckap1 depleted tumors also showed enhanced infiltration of CD4+, CD8+ and mast cells, perhaps representing an anti-tumor response and contributing to slow growth. CD4+ and

CD8⁺ are anti-tumour T-cells. Mast cells have an unclear role in cutaneous melanoma, but are generally thought to be tumour suppressive (Mignogna et al., 2017). Mast cells carry granules of inflammatory mediators such as histamine, heparin and cytokines and can modulate the activity of macrophages, with some reporting suggesting they could have both tumour provoking and opposing roles (Komi and Redegeld, 2020).

Cutaneous melanomas with activating BRAF mutations occur in approximately 50% of patients and BRAF/MEK inhibitor combination therapies can give more than a 75% response rate, but also a high relapse rate (Rebecca et al., 2020). Immune therapies, such as anti-PD-1 and anti CTLA-4 are also useful, but the response rate is less than 40% (Rebecca et al., 2020). Targeting NCKAP1, or a component of the actin machinery downstream of Rac1 would be challenging, but might boost the anti-tumour immune response and slow tumour growth. Clearly, more studies are needed to determine whether the apparent feedback loop between Rac1- Scar/WAVE and cell cycle progression could be broken with inhibitors, to slow tumour growth and possibly to enhance immune infiltration (Model, Figure S9).

Materials and Methods

Transgenic mice and genotyping

All experiments were performed according to UK Home Office regulations and in compliance with EU Directive 2010/63 and the UK Animals (Scientific Procedures) Act 1986 and were previously approved by the Animal Welfare and Ethical Review Body (AWERB) of the University of Glasgow. Experiments were accompanied by a UK Home Office project licence

to the corresponding author (PE494BE48). *Nckap1^{ff}* mice generation and genotyping are described in Supplementary Materials online.

Preparation of tumor lysates

Tumor samples were weighed and equivalent amount of tumor pieces for each sample were lysed in RIPA (50 mM Tris-HCL, 150 mM NaCl, 1% NP-40 v/v and 0.25% w/v Na deoxycholate) with Halt protease inhibitor cocktail (Thermofisher A32963) and Halt phosphatase inhibitor cocktail (Thermofisher 78428) for 10 min on ice. Tumor samples were then homogenized with electronic homogenizer (Precellys24, Stretton Scientific Ltd) and clarified at 10,000g using centrifugation (4⁰C).

BrdU incorporation and in vivo proliferation assay

In vivo proliferation levels of tumors were measured using bromodeoxyuridine (BrdU) incorporation assay. Briefly, mice were injected with 250 µl of BrdU (Amersham Biosciences, NJ, USA) when the tumors reach endpoint (1.2 cm) and sacrificed after 2 hrs. Immunohistochemical staining for BrdU was then performed using an anti-BrdU antibody (BD Bioscience, Oxford, UK).

Immunohistochemistry

Formalin-fixed paraffin-embedded (FFPE) sections were processed by standard histology processing techniques as previously described (Li et al., 2012b). Details of the antibodies are listed in Supplementary Information.

Statistical analysis

All values expressed as mean \pm SEM and statistical analysis was performed using Prism8 (GraphPad). Unpaired t-test was used to find significance between two groups. The LogRank (Mantel cox) test was used to calculate survival distribution between samples.

Data Availability Statement

All original data are contained within this manuscript or are available upon reasonable request to the corresponding author.

Conflict of Interest

The authors state no conflict of interest.

Acknowledgments

We acknowledge CRUK Beatson Institute Core Services and Advanced Technologies (C596/A17196). We thank the members of the transgenic technology team of the CRUK Beatson Institute, Dr. David Stevenson and Dr. Sheila Bryson for their help with mouse genotyping. We also thank Dr Catherine Winchester for proofreading and editing, the members of the Machesky and Insall labs for their helpful comments and feedback. We also thank the members of the BSU team at Beatson Institute of Cancer Research for their help with animal maintenance. WE acknowledge CRUK A15673 awarded to LMM and A17196 and A21139 grants awarded to OJS. VP was funded by a CRUK PhD studentship (A25142).

Author contributions

Conceptualization and design: KS, AC, LMM; acquisition of data: KS; analysis and interpretation: KS, AC, VP, FJH, EM, CN; Materials support: DS, OJS; Drafting the manuscript: KS, LMM.

Journal Pre-proof

FIGURE LEGENDS**FIGURE 1. Loss of *Nckap1* delayed the onset and development of melanoma.**

(a-b) Representative images of induced melanoma in *Nckap1*^{wt/wt} and *Nckap1*^{ff} mice with the genetic background *Tyr::CreER*^{T2+}; *Braf*^{V600E+}; *Pten*^{wt/ff} at 56 days (8 weeks) post tamoxifen induction. Arrows point to nevi. **(c)** Number of primary tumors per mouse upon *Nckap1* loss (n=14 *Nckap1*^{wt/wt} and n=16 *Nckap1*^{ff} mice) **(d)** Tumor burden (tumor volume (mm³)) upon *Nckap1* loss (n=14 *Nckap1*^{wt/wt} and n=16 *Nckap1*^{ff} mice). **(e-f)** Representative images from Haematoxylin & Eosin (H&E) staining of tumors from *Nckap1*^{wt/wt} and *Nckap1*^{ff} mice. Scale bars are 500 μm. All error bars show Mean ± SEM. Tumor size is in mm³. Unpaired t-test. ***P* < 0.01; *****P* < 0.0001.

FIGURE 2. *Nckap1* is important for cell cycle progression and tumor growth.

(a) Quantification of percentage of BrdU positive nuclei/cells from *Nckap1*^{wt/wt} (n=5 mice) and *Nckap1*^{ff} (n=5 mice) endpoint tumors under the genetic background *Tyr::CreER*^{T2+}; *Braf*^{V600E+}; *Pten*^{wt/ff} and after a 2hrs BrdU pulse. **(b)** Representative images from BrdU staining. **(c)** Quantification of percentage of ki67 positive nuclei/cells from *Nckap1*^{wt/wt} (n=5) and *Nckap1*^{ff} (n=7) tumors from separate mice. **(d)** Representative images of ki67 staining. **(e)** Quantification of cyclinD1 positive nuclei/cells from *Nckap1*^{wt/wt} (n=8) and *Nckap1*^{ff} (n=8) tumors from separate mice. **(f)** Representative images of cyclinD1 staining. **(g)** Tumor growth curves of *Nckap1*^{wt/wt} (n=7) and *Nckap1*^{ff} (n=7) mice. All error bars show Mean ± SEM.

Tumor size is in mm^3 . Unpaired t-test. * $P < 0.05$; ** $P < 0.01$; *** $P < 0.001$; **** $P < 0.0001$; ns = not-significant. Scale bars are $100 \mu\text{m}$.

FIGURE 3. *Nckap1* is dispensable for dermal expansion but essential for melanoma progression.

(a) Days to naevus formation from *Nckap1*^{wt/wt} (n=15 mice) and *Nckap1*^{ff} (n=14 mice) (b) tumor formation in *Nckap1*^{wt/wt} (n=15 mice) and *Nckap1*^{ff} (n= 11 mice) skin post-tamoxifen induction under the genetic background *Tyr::CreER*^{T2+}; *Braf*^{V600E+}; *Pten*^{wt/f}. (c-d) H&E staining showing pigmented lesions from *Nckap1*^{wt/wt} and *Nckap1*^{ff} end-point skin. Arrows – dermal lesions. (e) Quantification of pigmented dermis lesions from *Nckap1*^{wt/wt} (n=8 mice) and *Nckap1*^{ff} (n=6 mice) end-point skins post-tamoxifen induction. (f) Kaplan-Meier survival curve of mice with the indicated genotypes, *Nckap1*^{wt/wt} (n=16 mice), *Nckap1*^{f/wt} (n=12 mice) and *Nckap1*^{ff} (n=21 mice) under the genetic background of the *Tyr::CreER*^{T2+}; *Braf*^{V600E+}; *Pten*^{wt/f} following local administration of tamoxifen. Log-Rank (Mantel-Cox) test of survival plot revealed a significant difference ($p < 0.0001$) between *Nckap1*^{wt/wt} and *Nckap1*^{ff} genotypes. All error bars show Mean \pm SEM. Unpaired t-test. * $P < 0.05$; ** $P < 0.01$; *** $P < 0.001$. Scale bars are $200 \mu\text{m}$.

FIGURE 4. *Nckap1* loss promotes fibrosis in melanomas.

Representative images of Picro Sirius Red staining from *Nckap1*^{wt/wt} (a) and *Nckap1*^{ff} (b) end-point tumor sections under the genetic background of *Tyr::CreER*^{T2+}; *Braf*^{V600E+}; *Pten*^{wt/f}. (c) Quantification of percentage Picro Sirius Red positive area/ mm^2 from *Nckap1*^{wt/wt} (n=7) and *Nckap1*^{ff} (n=6) end-point tumor sections from separate mice. (d-e) Decay curves of

collagen structure (correlation) **(d)** and abundance (homogeneity) **(e)**. Values are average intensity \pm SEM (y-axis) as a function of distance (μm , x-axis) from tumor sections of *Nckap1*^{wt/wt} (n=11) and *Nckap1*^{ff} (n=11) mice quantified using two-photon microscopy. **(f)** Percentage of α -SMA positive area/ mm^2 in *Nckap1*^{wt/wt} (n=8) and *Nckap1*^{ff} (n=8) tumors from separate mice. All error bars show Mean \pm SEM. Unpaired t-test. ns = not-significant. Scale bars are 100 μm .

FIGURE 5. Increased expression of HIF1 α and reduced vascularization upon *Nckap1* loss.

Serial sections of *Nckap1*^{wt/wt} stained for **(a)** S100, **(b)** HIF1 α and **(c)** CD31. Inset shows magnification of area pointed by an arrow. **(d-f)** *Nckap1*^{ff} serial sections showing **(d)** S100, Tumor cells indicated by asterisk **(e)** HIF1 α and **(f)** CD31. *Nckap1*^{wt/wt} and *Nckap1*^{ff} mice are under the genetic background of *Tyr::CreER*^{T2+}; *Braf*^{V600E+}; *Pten*^{wt/f}. **(g)** Quantification showing percentage of HIF1 α positive areas/ mm^2 from *Nckap1*^{wt/wt} (n=7) and *Nckap1*^{ff} (n=7) tumors from separate mice. **(h)** Quantification of CD31 positive areas/ mm^2 from *Nckap1*^{wt/wt} (n=9) and *Nckap1*^{ff} (n=9) tumors from separate mice. **(i-j)** Representative images of TUNEL (cell death) staining in *Nckap1*^{wt/wt} and *Nckap1*^{ff} mice. Insets show magnification. **(k)** Quantification of TUNEL positive nuclei/ mm^2 from *Nckap1*^{wt/wt} (n=5) and *Nckap1*^{ff} (n=5) endpoint tumors from separate mice. All error bars show mean \pm SEM. Unpaired t-test. ***P* < 0.01; ****P* < 0.001; ns = not-significant. Scale bars are 100 μm .

FIGURE 6. *Nckap1* loss enhances immune infiltration in melanoma.

(a-b) Representative images from anti-CD8 (T-cells) staining from *Nckap1*^{wt/wt} and *Nckap1*^{ff} tumors under the genetic background of *Tyr::CreER*^{T2+}; *Braf*^{V600E+}; *Pten*^{wt/f}. **(c)** Quantification of CD8 positive cells/mm² of *Nckap1*^{wt/wt} (n=7) and *Nckap1*^{ff} (n=7) tumors from separate mice. **(d-e)** Representative images of toluidine blue (mast cells) staining from *Nckap1*^{wt/wt} and *Nckap1*^{ff} tumors. **(f)** Quantification of toluidine blue positive cells/mm² from *Nckap1*^{wt/wt} (n=7) and *Nckap1*^{ff} (n=7) tumors from separate mice. **(g-h)** Representative images of F4/80 positive cells (macrophages) staining from *Nckap1*^{wt/wt} and *Nckap1*^{ff} tumors from separate mice. **(i)** Quantification of F4/80 positive cells/mm² from *Nckap1*^{wt/wt} (n=6) and *Nckap1*^{ff} (n=6) tumors from separate mice. All error bars show mean ± SEM. Unpaired t-test. **P* < 0.05; ***P* < 0.01; ns = not-significant. Scale bars are 100 μm.

References

- Bailey KL, Agarwal E, Chowdhury S, Luo J, Brattain MG, Black JD, et al. TGFbeta/Smad3 regulates proliferation and apoptosis through IRS-1 inhibition in colon cancer cells. PLoS One 2017;12(4):e0176096.
- Chalhoub N, Baker SJ. PTEN and the PI3-kinase pathway in cancer. Annu Rev Pathol 2009;4:127-50.
- Chen B, Chou HT, Brautigam CA, Xing W, Yang S, Henry L, et al. Rac1 GTPase activates the WAVE regulatory complex through two distinct binding sites. Elife 2017;6.

Damsky W, Micevic G, Meeth K, Muthusamy V, Curley DP, Santhanakrishnan M, et al.

mTORC1 activation blocks BrafV600E-induced growth arrest but is insufficient for melanoma formation. *Cancer Cell* 2015;27(1):41-56.

Dankort D, Curley DP, Cartlidge RA, Nelson B, Karnezis AN, Damsky WE, Jr., et al.

Braf(V600E) cooperates with Pten loss to induce metastatic melanoma. *Nat Genet* 2009;41(5):544-52.

DeWane ME, Kelsey A, Oliviero M, Rabinovitz H, Grant-Kels JM. Melanoma on chronically sun-damaged skin: Lentigo maligna and desmoplastic melanoma. *J Am Acad Dermatol* 2019;81(3):823-33.

Dhomen N, Reis-Filho JS, da Rocha Dias S, Hayward R, Savage K, Delmas V, et al.

Oncogenic Braf induces melanocyte senescence and melanoma in mice. *Cancer Cell* 2009;15(4):294-303.

Franco OE, Shaw AK, Strand DW, Hayward SW. Cancer associated fibroblasts in cancer pathogenesis. *Semin Cell Dev Biol* 2010;21(1):33-9.

Gilkes DM, Semenza GL, Wirtz D. Hypoxia and the extracellular matrix: drivers of tumour metastasis. *Nat Rev Cancer* 2014;14(6):430-9.

Girard CA, Lecacheur M, Ben Jouira R, Berestjuk I, Diazzi S, Prod'homme V, et al. A Feed-Forward Mechanosignaling Loop Confers Resistance to Therapies Targeting the MAPK Pathway in BRAF-Mutant Melanoma. *Cancer Res* 2020;80(10):1927-41.

Halaban R. RAC1 and melanoma. *Clin Ther* 2015;37(3):682-5.

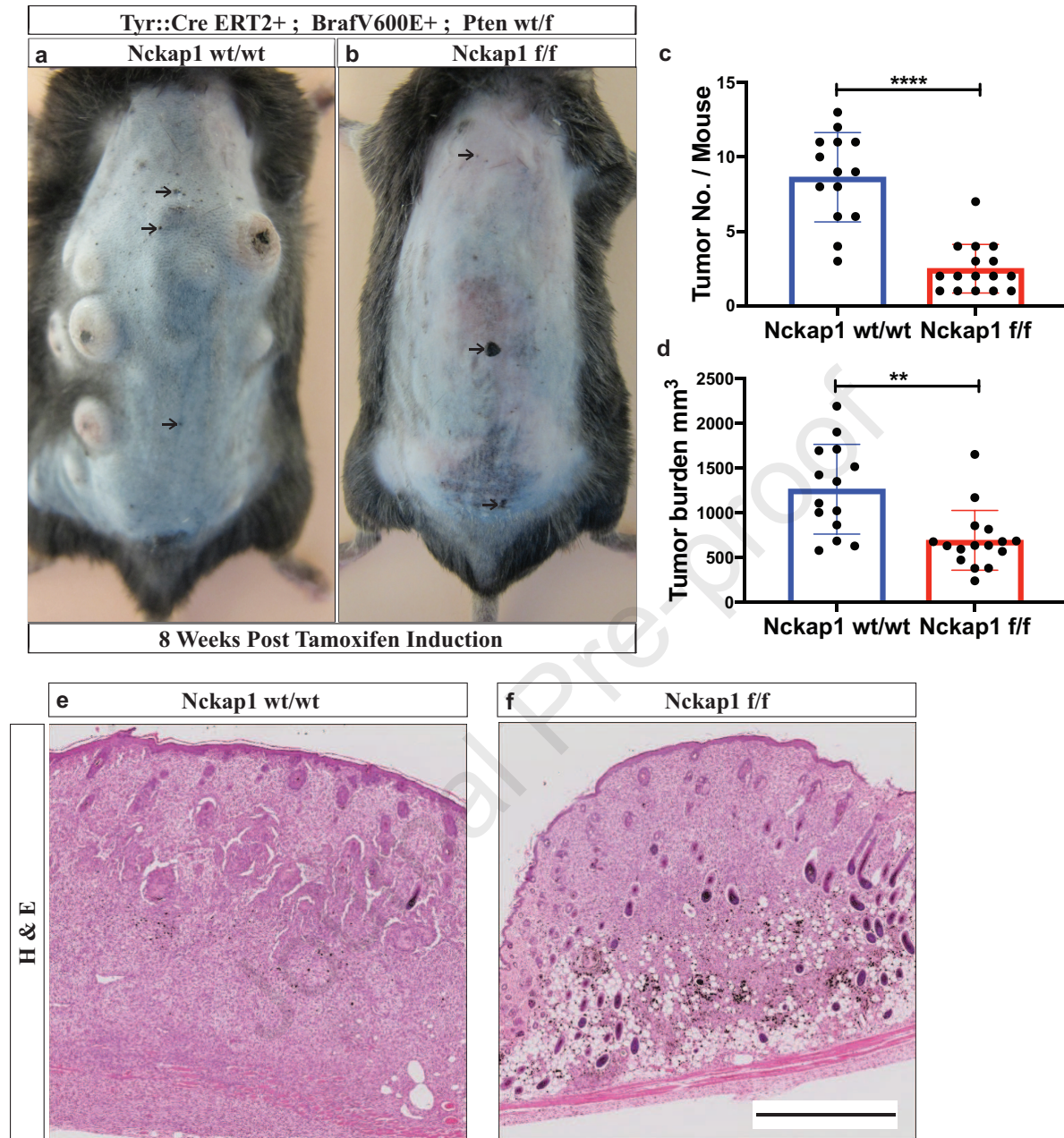
Hynes RO. The extracellular matrix: not just pretty fibrils. *Science* 2009;326(5957):1216-9.

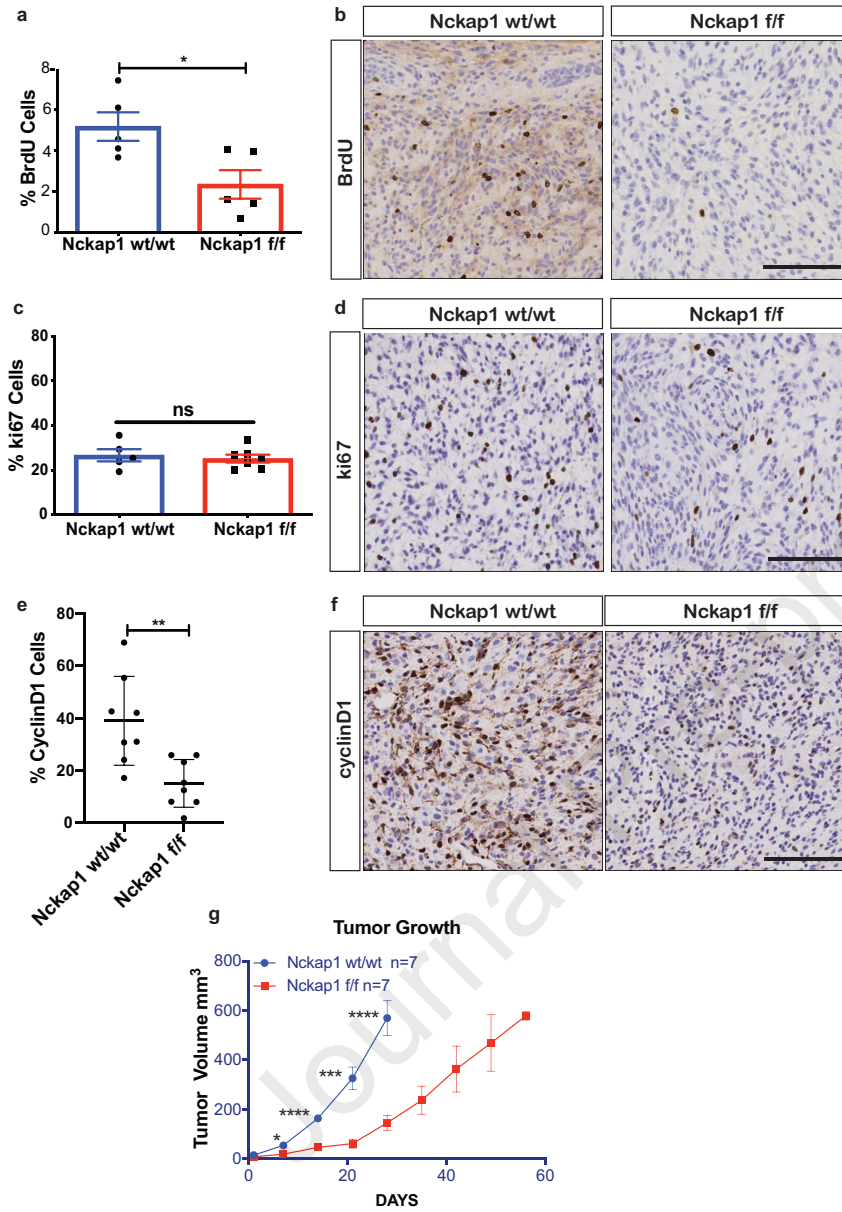
Ibarra N, Blagg SL, Vazquez F, Insall RH. Nap1 regulates Dictyostelium cell motility and adhesion through SCAR-dependent and -independent pathways. *Curr Biol* 2006;16(7):717-22.

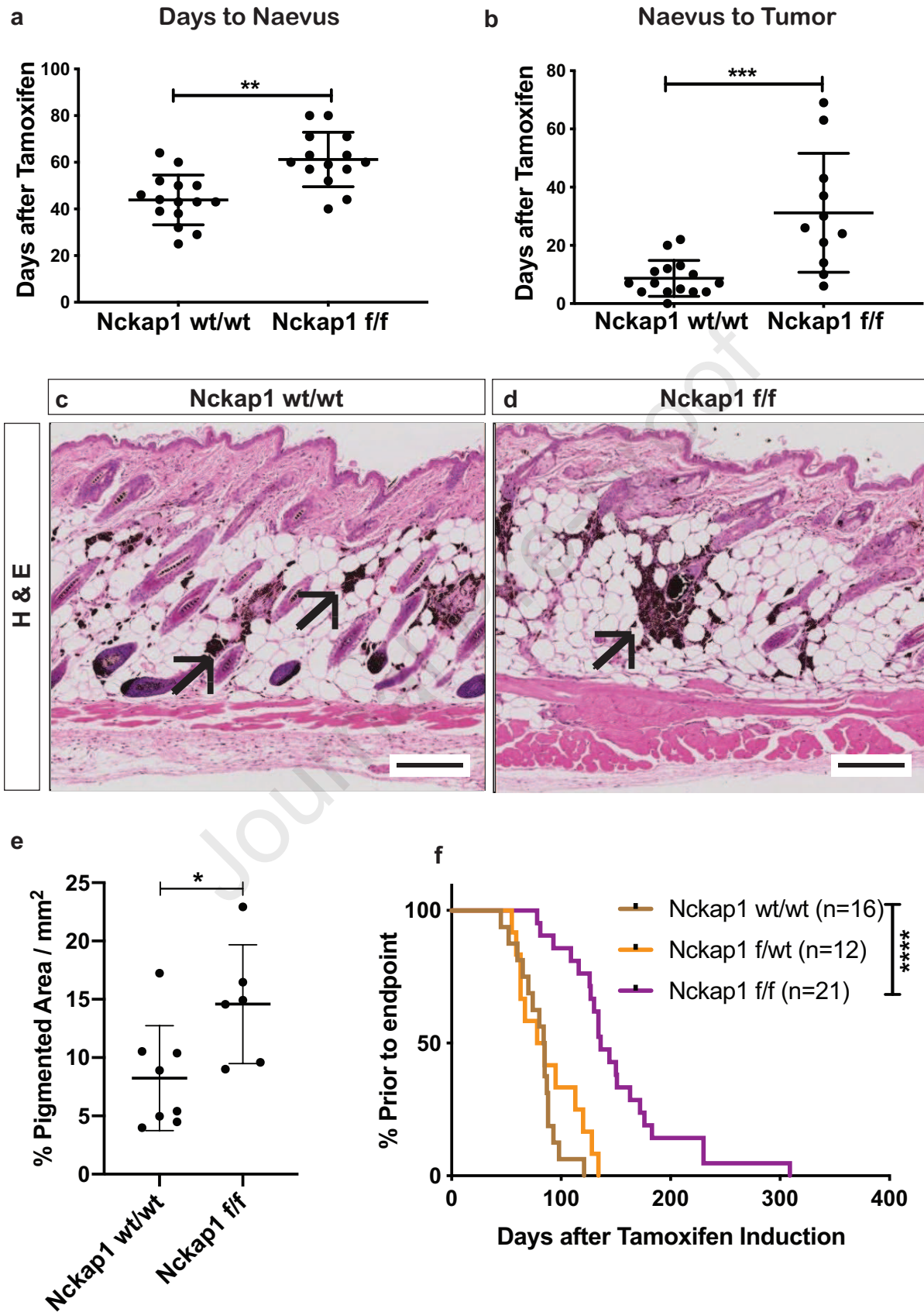
- Komi DEA, Redegeld FA. Role of Mast Cells in Shaping the Tumor Microenvironment. *Clin Rev Allergy Immunol* 2020;58(3):313-25.
- Laurette P, Coassolo S, Davidson G, Michel I, Gambi G, Yao W, et al. Chromatin remodellers Brg1 and Bptf are required for normal gene expression and progression of oncogenic Braf-driven mouse melanoma. *Cell Death Differ* 2020;27(1):29-43.
- Li A, Ma Y, Jin M, Mason S, Mort RL, Blyth K, et al. Activated mutant NRas(Q61K) drives aberrant melanocyte signaling, survival, and invasiveness via a Rac1-dependent mechanism. *J Invest Dermatol* 2012;132(11):2610-21.
- Li A, Ma Y, Yu X, Mort RL, Lindsay CR, Stevenson D, et al. Rac1 drives melanoblast organization during mouse development by orchestrating pseudopod- driven motility and cell-cycle progression. *Dev Cell* 2011;21(4):722-34.
- Li A, Machesky LM. Rac1 cycling fast in melanoma with P29S. *Pigment Cell Melanoma Res* 2013.
- Lionarons DA, Hancock DC, Rana S, East P, Moore C, Murillo MM, et al. RAC1(P29S) Induces a Mesenchymal Phenotypic Switch via Serum Response Factor to Promote Melanoma Development and Therapy Resistance. *Cancer Cell* 2019;36(1):68-83 e9.
- Lu P, Weaver VM, Werb Z. The extracellular matrix: a dynamic niche in cancer progression. *J Cell Biol* 2012;196(4):395-406.
- Magin TM, McWhir J, Melton, DW. A New Mouse Embryonic Stem cell Line With Good Germ Line Contribution and Gene Targeting Frequency. *Nucleic Acids Res.* 1992, 20, 3795–3796.
- Merlino G, Herlyn M, Fisher DE, Bastian BC, Flaherty KT, Davies MA, et al. The state of melanoma: challenges and opportunities. *Pigment Cell Melanoma Res* 2016;29(4):404-16.

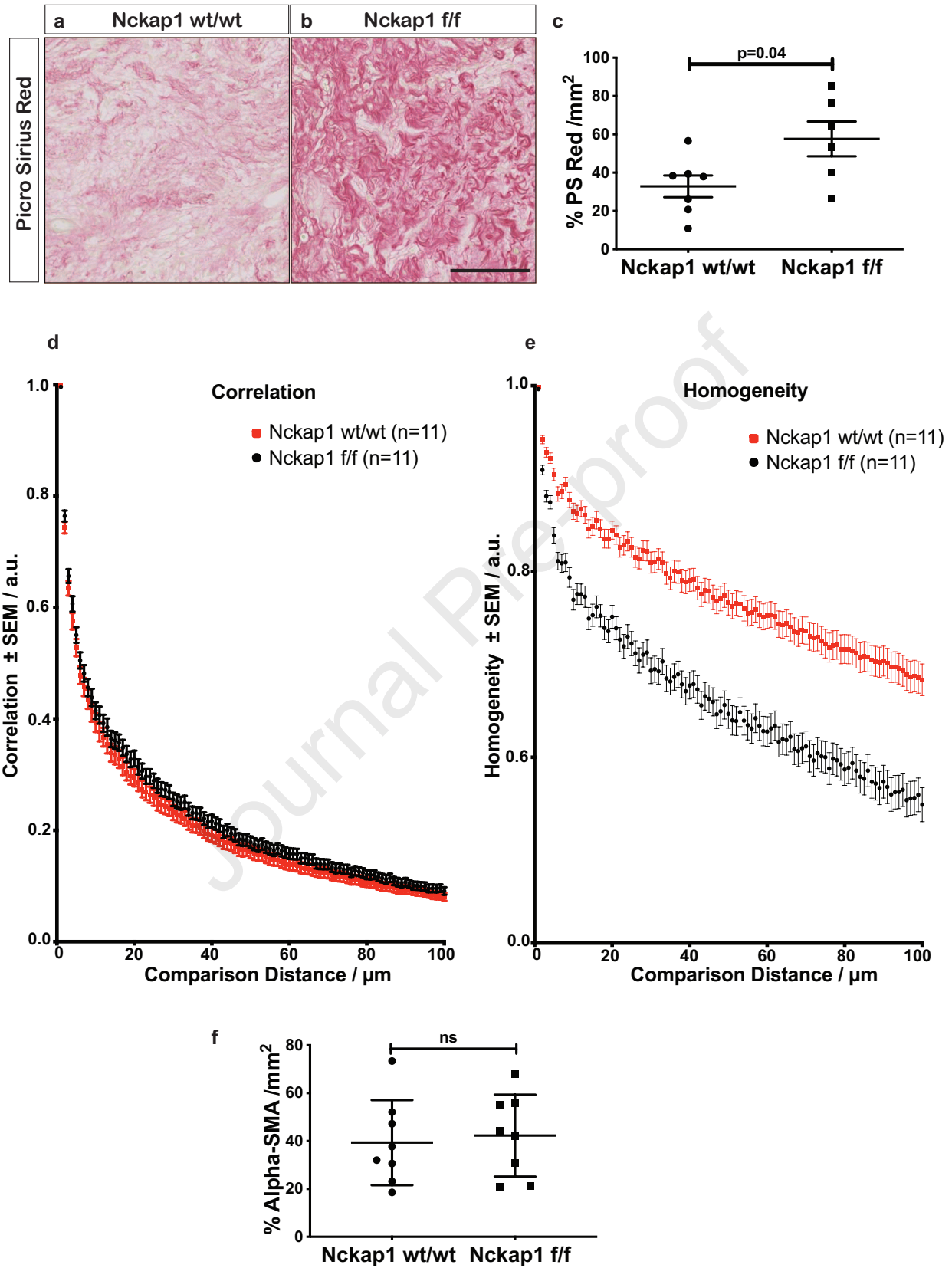
- Mignogna C, Scali E, Camastra C, Presta I, Zeppa P, Barni T, et al. Innate immunity in cutaneous melanoma. *Clin Exp Dermatol* 2017;42(3):243-50.
- Miskolczi Z, Smith MP, Rowling EJ, Ferguson J, Barriuso J, Wellbrock C. Collagen abundance controls melanoma phenotypes through lineage-specific microenvironment sensing. *Oncogene* 2018;37(23):3166-82.
- Molinie N, Rubtsova SN, Fokin A, Visweshwaran SP, Rocques N, Polesskaya A, et al. Cortical branched actin determines cell cycle progression. *Cell Res* 2019;29(6):432-45.
- Naba A, Clauser KR, Ding H, Whittaker CA, Carr SA, Hynes RO. The extracellular matrix: Tools and insights for the "omics" era. *Matrix Biol* 2016;49:10-24.
- Nagy A, Behringer R, Gertsenstein M, Nagy KV. *Manipulating the Mouse Embryo: A Laboratory Manual*, 3rd ed.; Brownstein, D.G., Ed.; Cold Spring Harbour Laboratory Press: Suffolk County, NY, USA, 2003; Volume 78.
- Perez-Guijarro E, Day CP, Merlino G, Zaidi MR. Genetically engineered mouse models of melanoma. *Cancer* 2017;123(S11):2089-103.
- Pollitt AY, Insall RH. WASP and SCAR/WAVE proteins: the drivers of actin assembly. *J Cell Sci* 2009;122(Pt 15):2575-8.
- Rainero E, Howe JD, Caswell PT, Jamieson NB, Anderson K, Critchley DR, et al. Ligand-Occupied Integrin Internalization Links Nutrient Signaling to Invasive Migration. *Cell Rep* 2015;10(3):398-413.
- Rath N, Morton JP, Julian L, Helbig L, Kadir S, McGhee EJ, et al. ROCK signaling promotes collagen remodeling to facilitate invasive pancreatic ductal adenocarcinoma tumor cell growth. *EMBO Mol Med* 2017;9(2):198-218.
- Rebecca VW, Somasundaram R, Herlyn M. Pre-clinical modeling of cutaneous melanoma. *Nat Commun* 2020;11(1):2858.

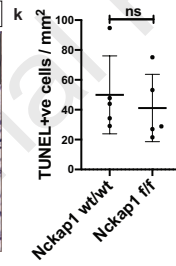
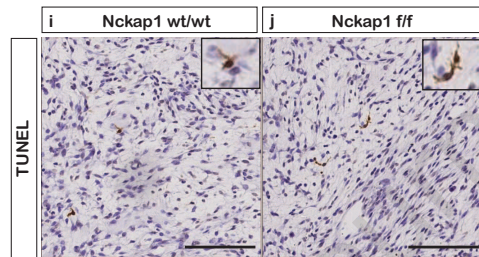
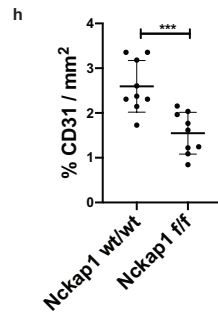
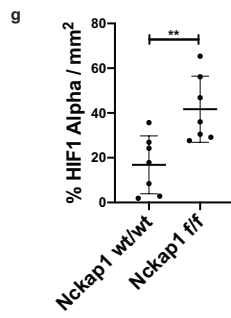
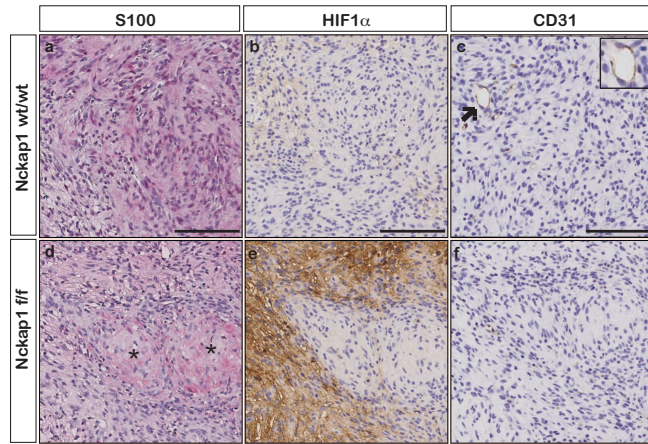
- Steffen A, Rottner K, Ehinger J, Innocenti M, Scita G, Wehland J, et al. Sra-1 and Nap1 link Rac to actin assembly driving lamellipodia formation. *EMBO J* 2004;23(4):749-59.
- Stradal TE, Rottner K, Disanza A, Confalonieri S, Innocenti M, Scita G. Regulation of actin dynamics by WASP and WAVE family proteins. *Trends Cell Biol* 2004;14(6):303-11.
- Suzuki A, Yamaguchi MT, Ohteki T, Sasaki T, Kaisho T, Kimura Y, et al. T cell-specific loss of Pten leads to defects in central and peripheral tolerance. *Immunity* 2001;14(5):523-34.
- Tang H, Li A, Bi J, Veltman DM, Zech T, Spence HJ, et al. Loss of Scar/WAVE complex promotes N-WASP- and FAK-dependent invasion. *Curr Biol* 2013;23(2):107-17.
- Watson IR, Li L, Cabeceiras PK, Mahdavi M, Gutschner T, Genovese G, et al. The RAC1 P29S hotspot mutation in melanoma confers resistance to pharmacological inhibition of RAF. *Cancer Res* 2014;74(17):4845-52.
- Yang K, Mahalingam M. Differing biologic behaviors of desmoplastic melanoma subtypes: Insights based on histopathologic, immunohistochemical, and genetic analyses. *J Am Acad Dermatol* 2020.

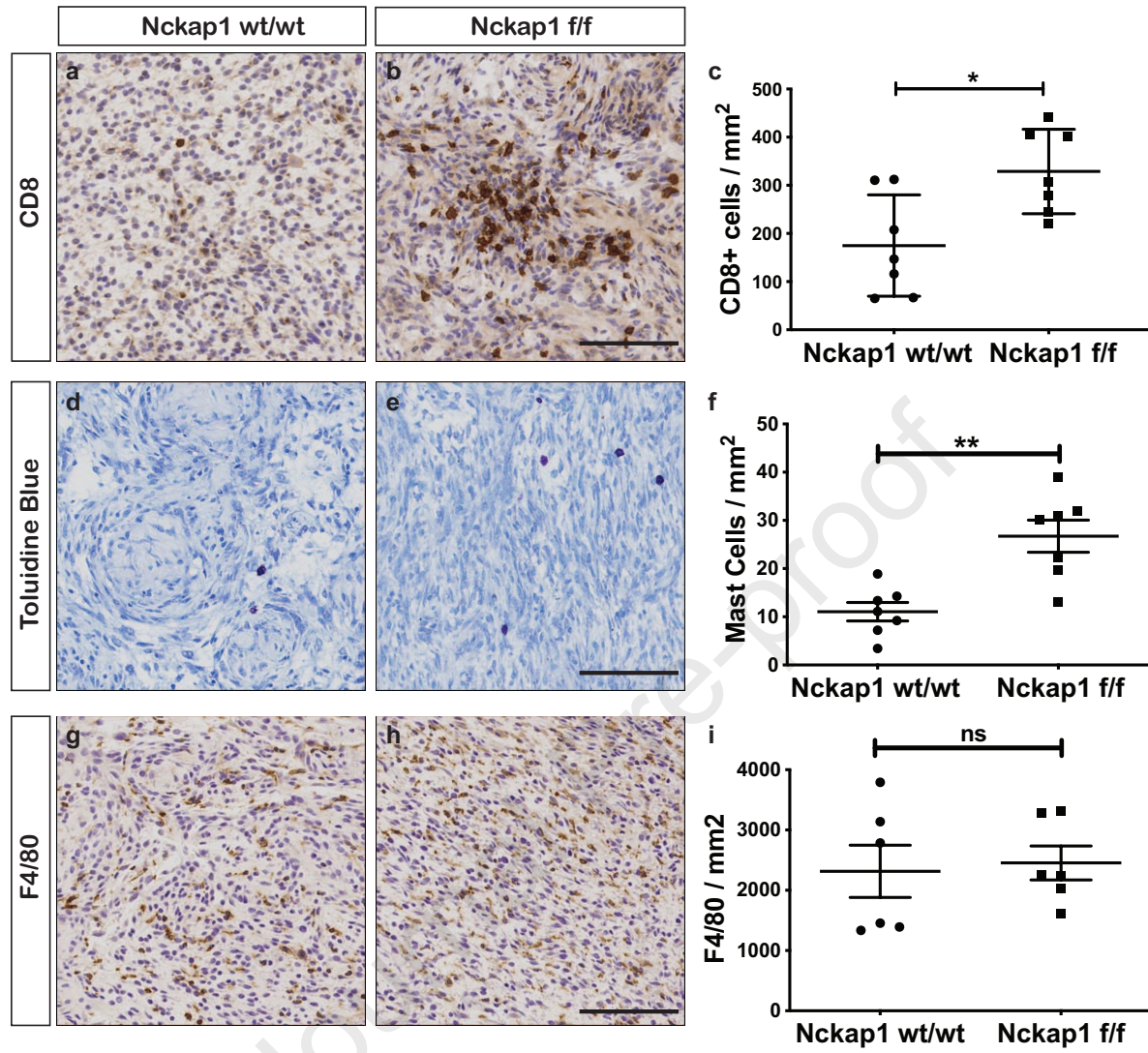












Proteome profiler Mouse XL Cytokine Array (ARY028) coordinates

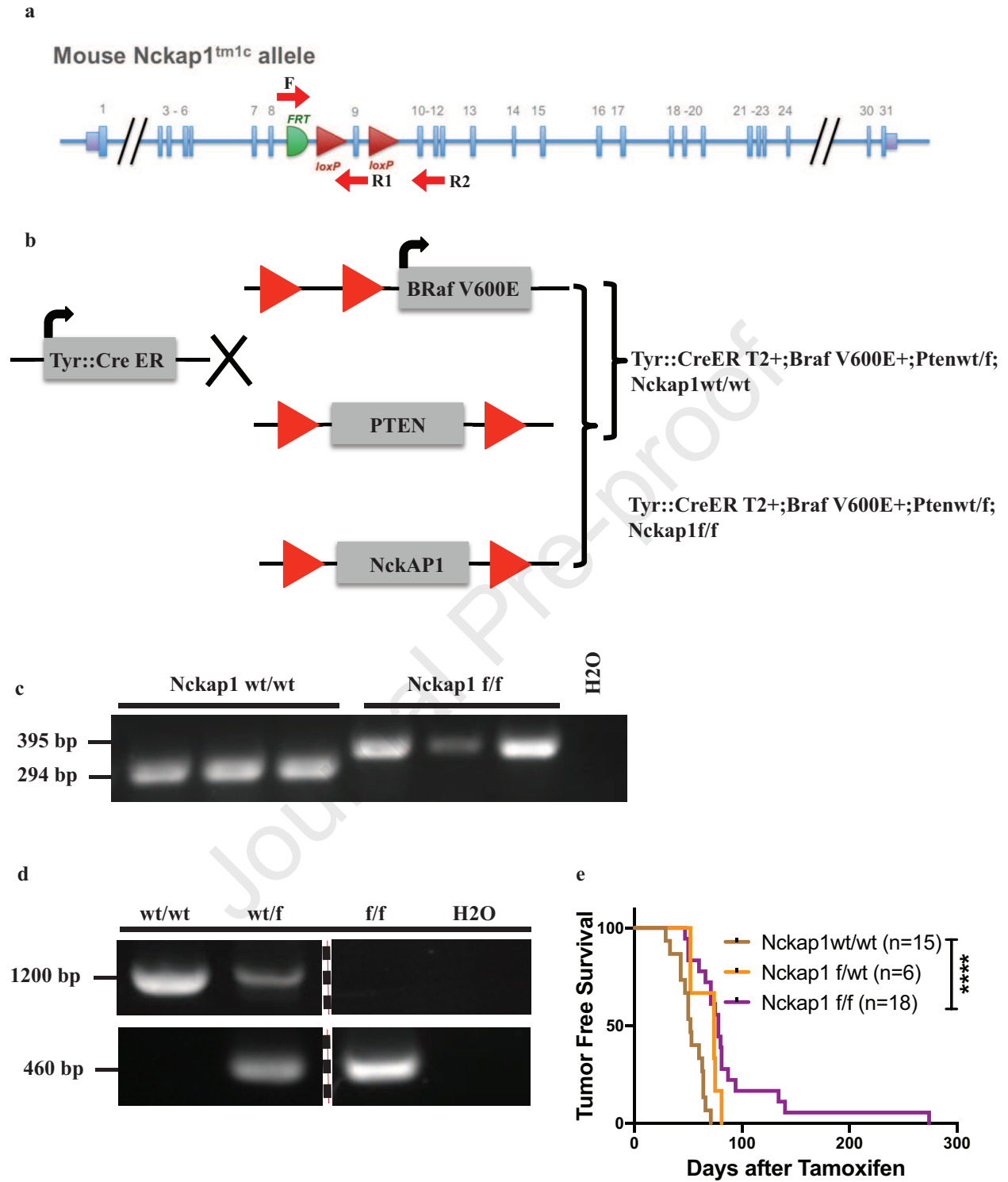
Coordinate	Analyte/Control	Entrez Gene ID	Alternate Nomenclature
A1, A2	Reference Spots	N/A	_____
A3, A4	Adiponectin/Acrp30	11450	AdipoQ
A5, A6	Amphiregulin	11839	AR, SDGF
A7, A8	Angiopoietin-1	11600	Ang-1, Angpt1
A9, A10	Angiopoietin-2	11601	Ang-2, Angpt2
A11, A12	Angiopoietin-like 3	30924	ANGPT-L3
A13, A14	BAFF/BLYS/TNFSF13B	24099	CD257, TALL1, THANK, ZTNF4
A15, A16	C1q R1/CD93	17064	AA4 Antigen, C1q Rp, CD93
A17, A18	CCL2/JE/MCP-1	20296	MCAF
A19, A20	CCL3/CCL4/MIP-1 α / β	20302/20303	_____
A21, A22	CCL5/RANTES	20304	SISd
A23, A24	Reference Spots	N/A	_____
B3, B4	CCL6/C10	20305	MRP-1
B5, B6	CCL11/Eotaxin	20292	_____
B7, B8	CCL12/MCP-5	20293	_____
B9, B10	CCL17/TARC	20295	_____
B11, B12	CCL19/MIP-3 β	24047	ELC
B13, B14	CCL20/MIP-3 α	20297	exodus-1, LARC
B15, B16	CCL21/6Ckine	18829	exodus-2, SCYA21, SLC, TCA-4
B17, B18	CCL22/MDC	20299	ABCD-1, MDC, STCP-1
B19, B20	CD14	12475	_____
B21, B22	CD40/TNFRSF5	21939	_____
C3, C4	CD160	54215	Natural killer cell receptor BY55, NK1; NK28
C5, C6	Chemerin	71660	RARRES2, TIG-2
C7, C8	Chitinase 3-like 1	12654	CHI3L1, Cgp39, YKL40
C9, C10	Coagulation Factor III/Tissue Factor	14066	TF, CD142, Thromboplastin
C11, C12	Complement Component C5/C5a	15139	C5/C5a
C13, C14	Complement Factor D	11537	Adipsin, C3 convertase activator, Properdin factor D
C15, C16	C-Reactive Protein/CRP	12944	_____
C17, C18	CX3CL1/Fractalkine	20312	FKN, Neurotactin
C19, C20	CXCL1/KC	14825	CINC-1; GRO alpha; KC; MGSA-alpha
C21, C22	CXCL2/MIP-2	20310	GRO β , GRO2, CINC-3
D1, D2	CXCL9/MIG	17329	CRG-10, CMK
D3, D4	CXCL10/IP-10	15945	CRG-2, C7
D5, D6	CXCL11/I-TAC	56066	H174, SCYB9B
D7, D8	CXCL13/BLC/BCA-1	55985	_____
D9, D10	CXCL16	66102	SRPSOX
D11, D12	Cystatin C	13010	ARMD11, CST3, Gamma-trace
D13, D14	DKK-1	13380	Dickkopf-1
D15, D16	DPPIV/CD26	13482	Dpp4, Dipeptidyl-peptidase IV
D17, D18	EGF	13645	Epidermal Growth Factor
D19, D20	Endoglin/CD105	13805	ENG
D21, D22	Endostatin	12822	Col18a1
D23, D24	Fetuin A/AHSG	11625	AHSG, alpha-2-HS-glycoprotein
E1, E2	FGF acidic	14164	FGF-1
E3, E4	FGF-21	56636	_____
E5, E6	Flt-3 Ligand	14256	Flt3lg
E7, E8	Gas 6	14456	Growth Arrest Specific
E9, E10	G-CSF	12985	Csf3
E11, E12	GDF-15	23886	MIC-1

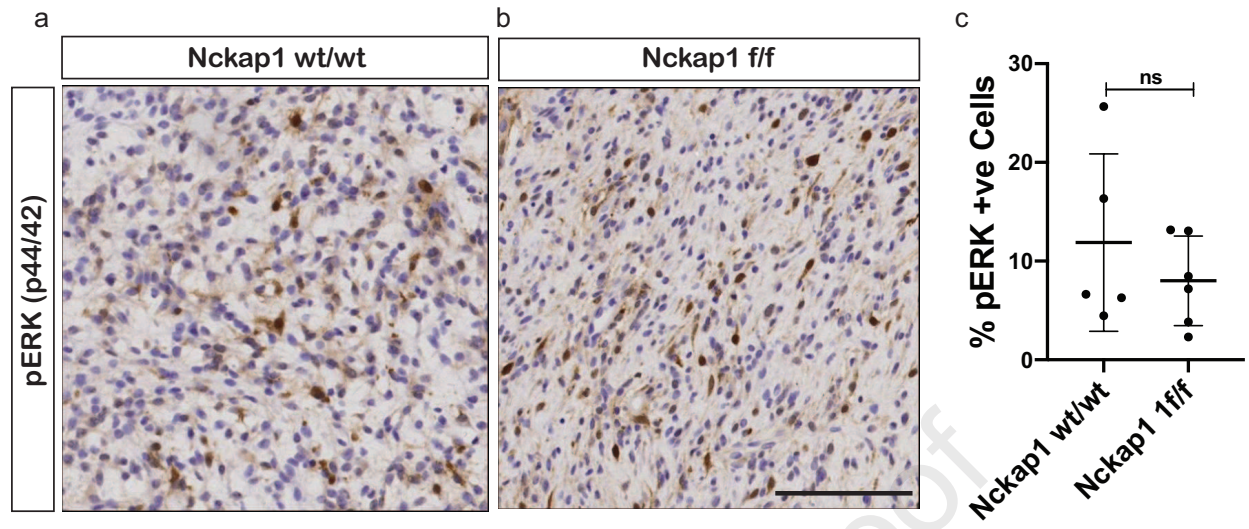
E			
E15, E16	HGF	15234	Scatter Factor, SF, Hepatopoietin-A
E17, E18	ICAM-1/CD54	15894	_____
E19, E20	IFN- γ	15978	IFNG
E21, E22	IGFBP-1	16006	_____
E23, E24	IGFBP-2	16008	_____
F1, F2	IGFBP-3	16009	_____
F3, F4	IGFBP-5	16011	_____
F5, F6	IGFBP-6	16012	_____
F7, F8	IL-1 α /IL-1F1	16175	_____
F9, F10	IL-1 β /IL-1F2	16176	_____
F11, F12	IL-1ra/IL-1F3	16181	IL1RN
F13, F14	IL-2	16183	_____
F15, F16	IL-3	16187	_____
F17, F18	IL-4	16189	B cell-stimulatory factor-1
F19, F20	IL-5	16191	_____
F21, F22	IL-6	16193	_____
F23, F24	IL-7	16196	_____
G1, G2	IL-10	16153	CSIF
G3, G4	IL-11	16156	_____
G5, G6	IL-12 p40	16160	_____
G7, G8	IL-13	16163	_____
G9, G10	IL-15	16168	_____
G11, G12	IL-17A	16171	_____
G13, G14	IL-22	50929	IL-TIF
G15, G16	IL-23	83430	_____
G17, G18	IL-27 p28	246779	_____
G19, G20	IL-28A/B	330496/338374	_____
G21, G22	IL-33	77125	NF HEV, DVS 27
G23, G24	LDL R	16835	low density lipoprotein receptor
H1, H2	Leptin	16846	OB
H3, H4	LIF	16878	_____
H5, H6	Lipocalin-2/NGAL	16819	Siderocalin, 24p3
H7, H8	LIX	20311	CXCL5, GCP-2, ENA-78
H9, H10	M-CSF	12977	CSF-1
H11, H12	MMP-2	17390	Gelatinase A
H13, H14	MMP-3	17392	Stromelysin-1
H15, H16	MMP-9	17395	Clg4b, Gelatinase B, GELB
H17, H18	Myeloperoxidase	17523	MPO
H19, H20	Osteopontin (OPN)	20750	Eta-1, Spp1
H21, H22	Osteoprotegerin/TNFRSF11B	18383	OPG, Ocif
H23, H24	PD-ECGF/Thymidine phosphorylase	72962	dThdPase, ECGF1, Gliostatin, MEDPS1, MNGIE
I1, I2	PDGF-BB	18591	_____
I3, I4	Pentraxin 2/SAP	20219	PTX2
I5, I6	Pentraxin 3/TSG-14	19288	PTX3
I7, I8	Periostin/OSF-2	50706	Fasciclin I-like, POSTN, TRIF52
I9, I10	Pref-1/DLK-1/FA1	13386	DLK1, pG2, ZOG
I11, I12	Proliferin	18811	MRP
I13, I14	Proprotein Convertase 9/PCSK9	100102	NARC-1
I15, I16	RAGE	11596	AGER
I17, I18	RBP4	19662	Retinol-Binding Protein 4
I19, I20	Reg3G	19695	PAP3
I21, I22	Resistin	57264	ADSF, FIZZ3

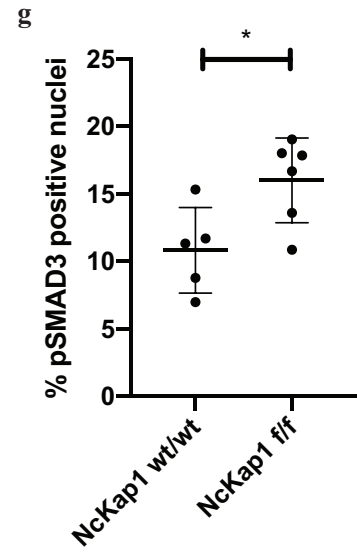
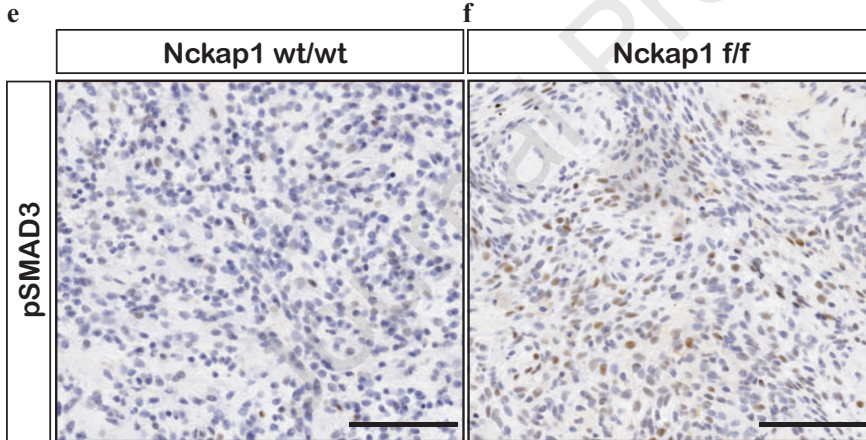
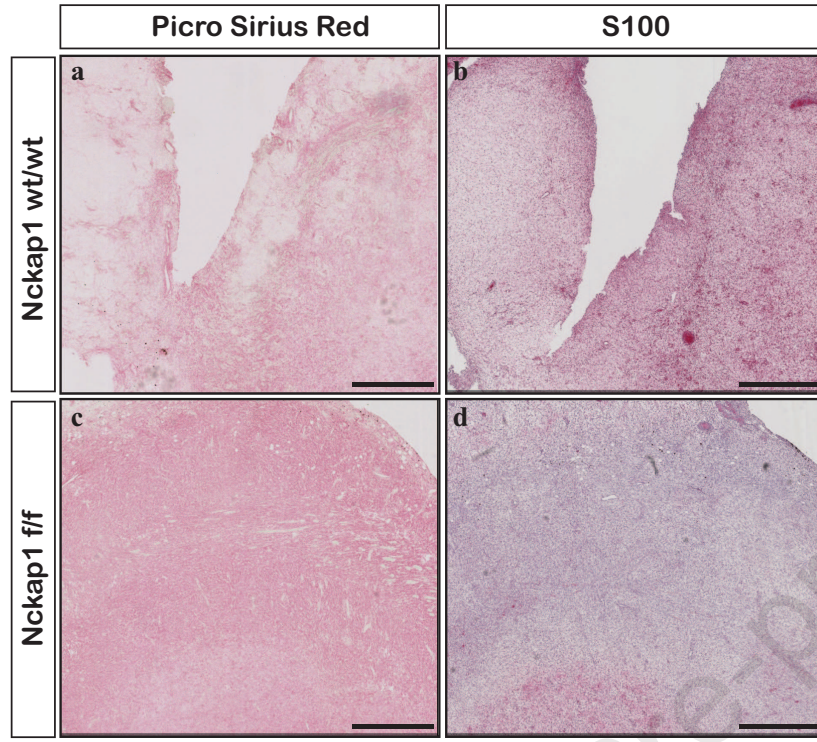
J3, J4	E-Selectin/CD62E	20339	ELAM1, LECAM2, Sele
J5, J6	P-Selectin/CD62P	20344	GMP-140, LECAM3, Selep
J7, J8	Serpin E1/PAI-1	18787	Nexin, PLANH1
J9, J10	Serpin F1/PEDF	20317	EPC-1
J11, J12	Thrombopoietin	21832	Tpo, MGDF
J13, J14	TIM-1/KIM-1/HAVCR	171283	_____
J15, J16	TNF- α	21926	TNFSF1A
J17, J18	VCAM-1/CD106	22329	_____
J19, J20	VEGF	22339	VEGF-A, VPF
J21, J22	WISP-1/CCN4	22402	_____
J23, J24	Negative Control	N/A	_____

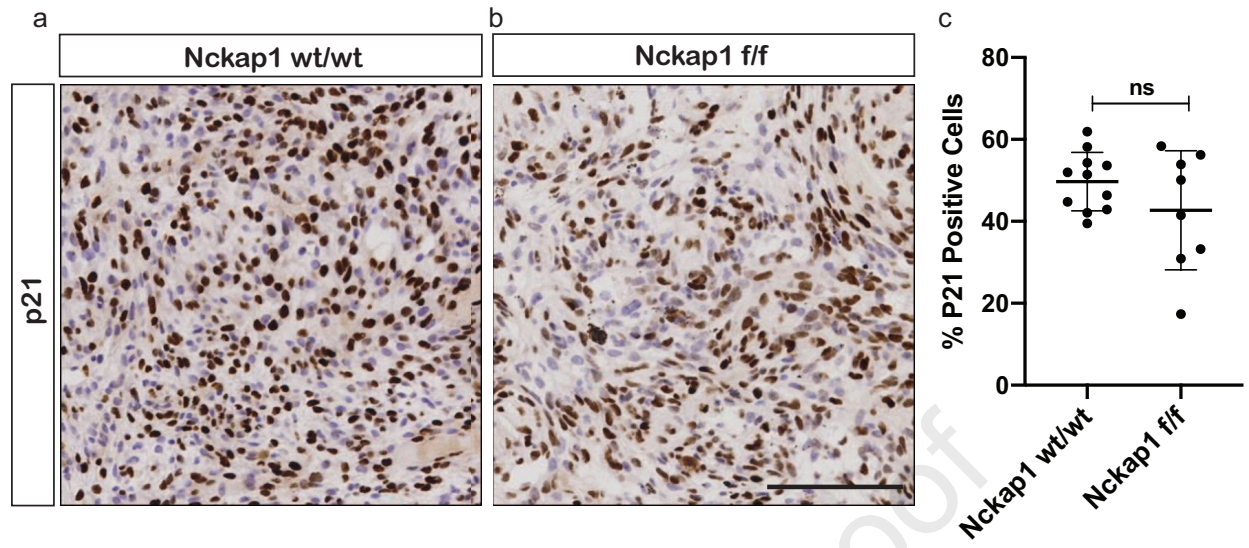
Table S2 Tumour Growth Data

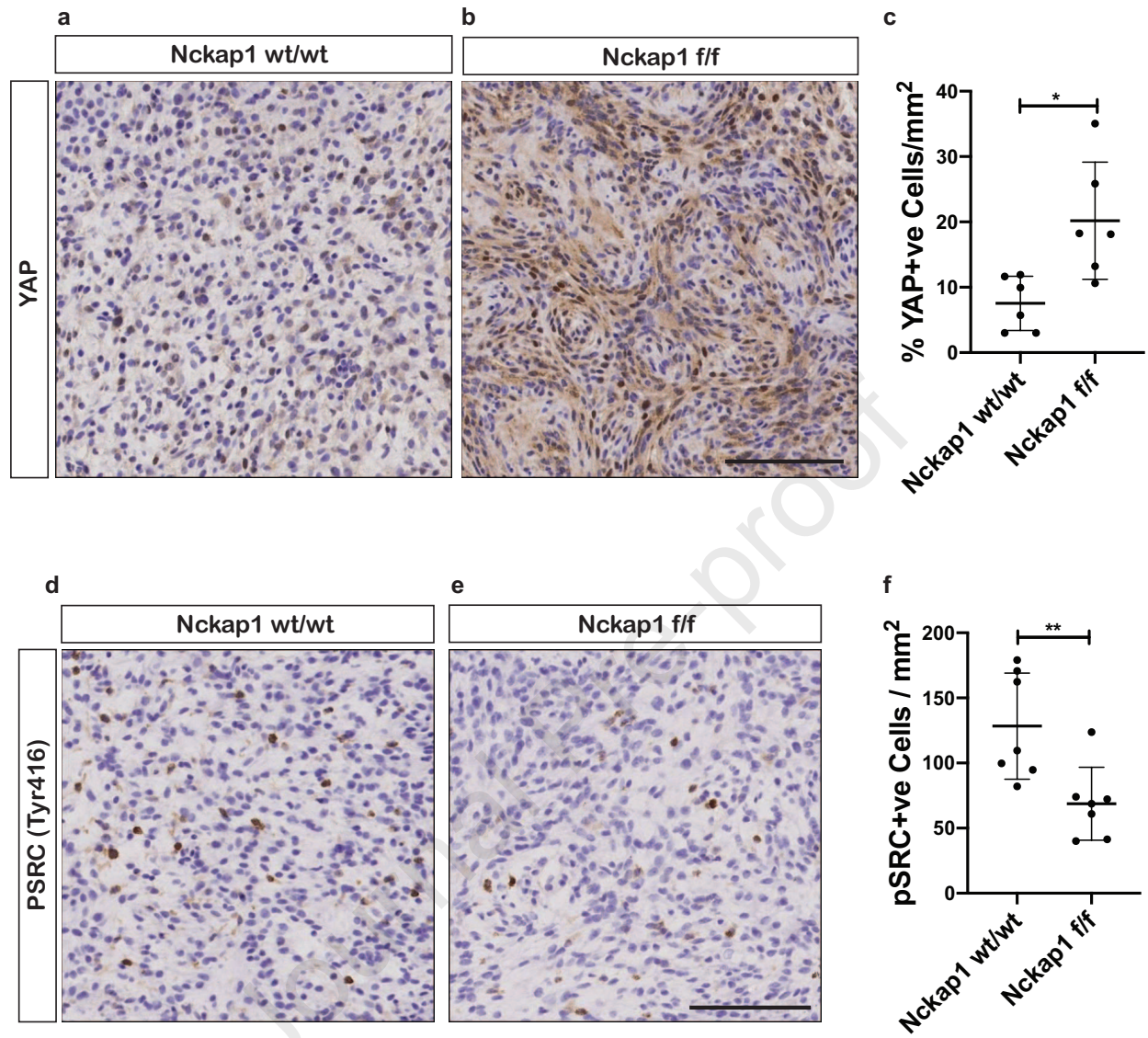
	BKSE3.1f	BKSE4.3a	BKSE6.3e	BKSE5.4c	BKSE11.1a	BKSE11.1f	BKSE12.1e
	Raw Values	Raw Values	Raw Values	Raw Values	Raw Values	Raw Values	Raw Values
Day1	May be 2.7x2.7	2.8x2.8	3.4x3.4	3.3x3.3	1.8x1.8	1.6x1.6	2(1x1)
Day7	4.3x4.3	4.3x4	3.6x3.5	4.5x4.5	2(3.1x3.1)	3x2.9	2.8x2.8
Day14	5.1x4	5.3x4.9	5.6x5.4	5.4x4.9	4.6x3.8	4.7x3.7	3.9x3.6
Day21	5.9x5.2	5.8x5.2	6.8x6.6		4.3x4.2	5.2x5	4.6x4
Day28	6.2x5.7	7.3x7.3	8.5x7.8	7.3x7	6.6x4.5	7.2x7.2	5.4x4.5
Day35	6.3x6.3	7.7x7.5	10x10	8.1x7.6	7.9x6.6	9.1x8.9	6.7x6.2
Day42	7.6x6.9	9.4x8.1	12.3x11.8	9.5x9.3	8.6x7.3	10x9.3	7x7
Day49	9.4x8.8	10.8x9.8		9.9x9.3		12x12	
Day56	10.8x10.2	11x10.4					
Day63							
Day70							
Day77							
	Tumor Volume	Tumor Volume	Tumor Volume	Tumor Volume	Tumor Volume	Tumor Volume	Tumor Volume
Day1	9.8415	2.8	19.652	17.9685	2.916	2.048	0.5
Day7	39.7535	4	22.05	45.5625	14.8955	12.615	10.976
Day14	40.8	63.6265	81.648	64.827	33.212	32.1715	25.272
Day21	79.768	78.416	148.104	0	37.926	65	36.8
Day28	100.719	194.5085	258.57	178.85	66.825	186.624	54.675
Day35	125.0235	216.5625	500	233.928	172.062	360.4055	128.774
Day42	180.918	308.367	856.326	410.8275	229.1	432.45	171.5
Day49	363.968	518.616		428.1255		864	
Day56	561.816	594.88					
Day63							
Day70							
Day77							

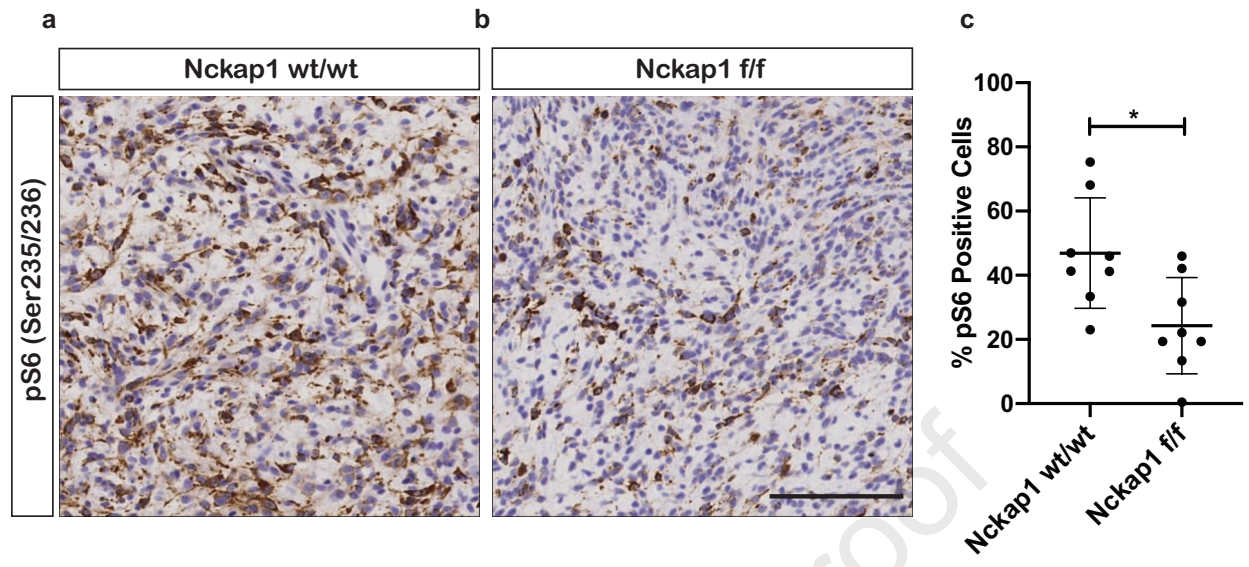


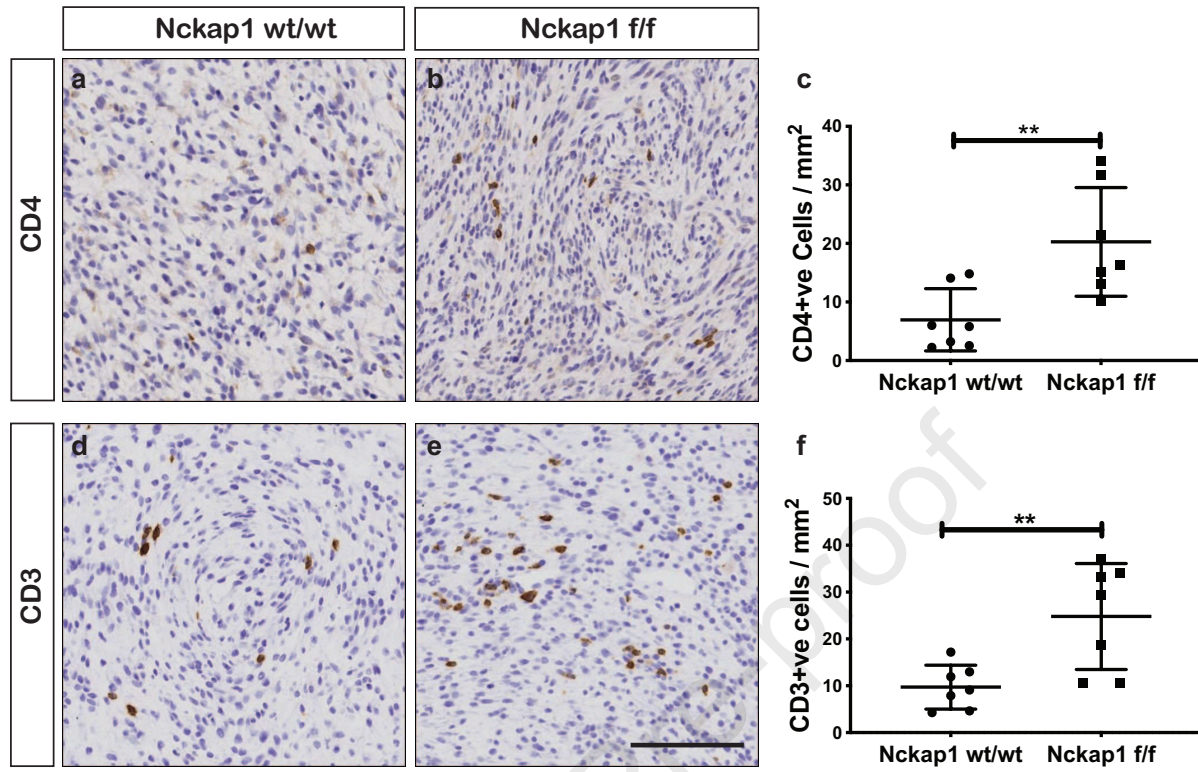


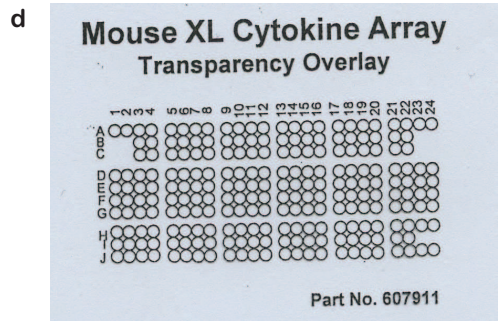
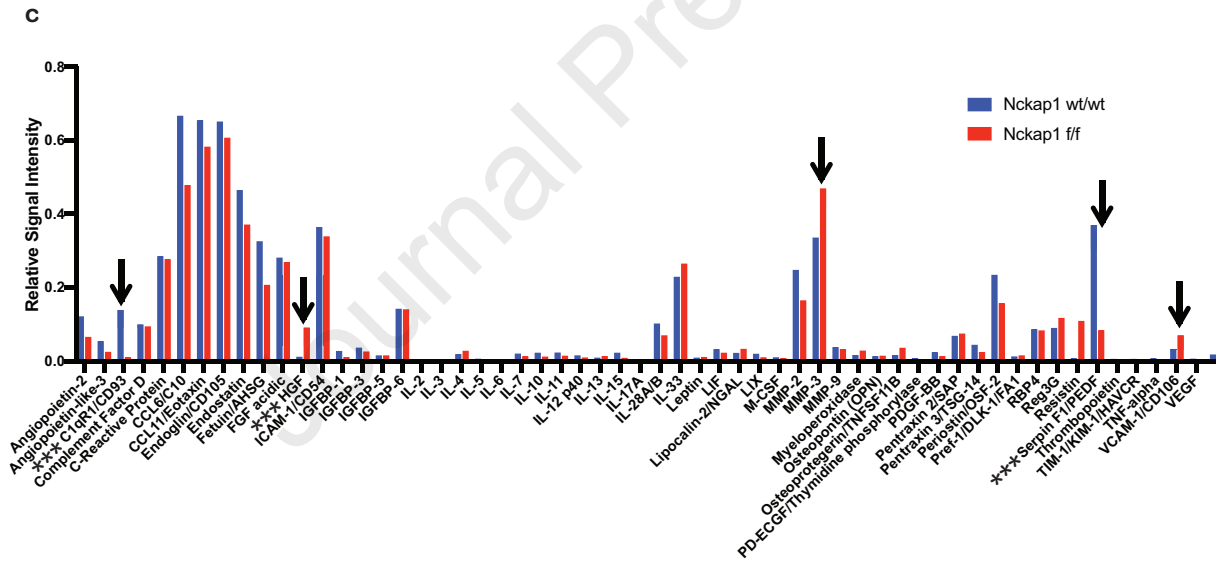
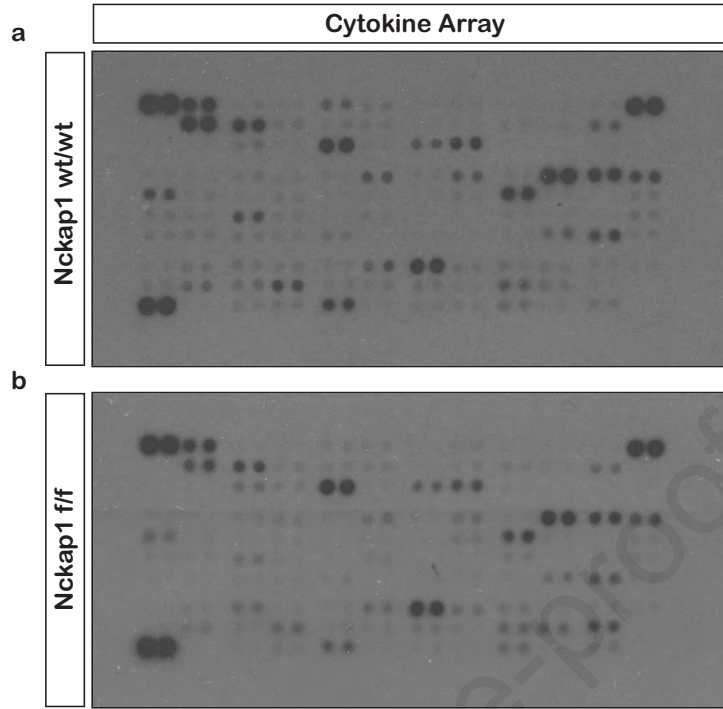




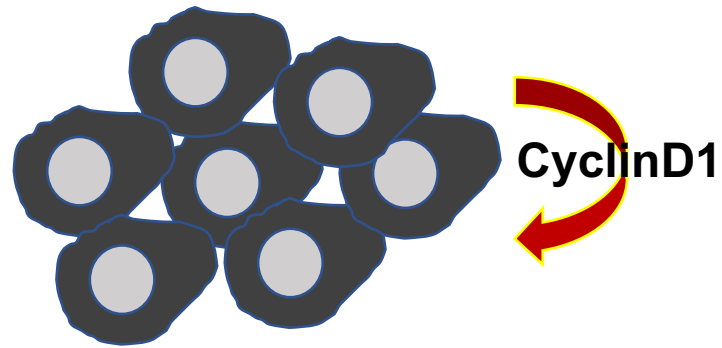
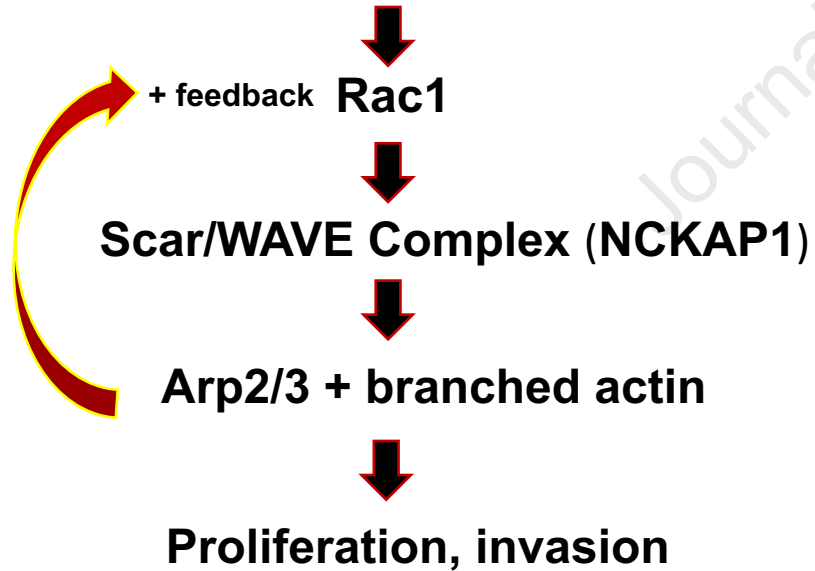




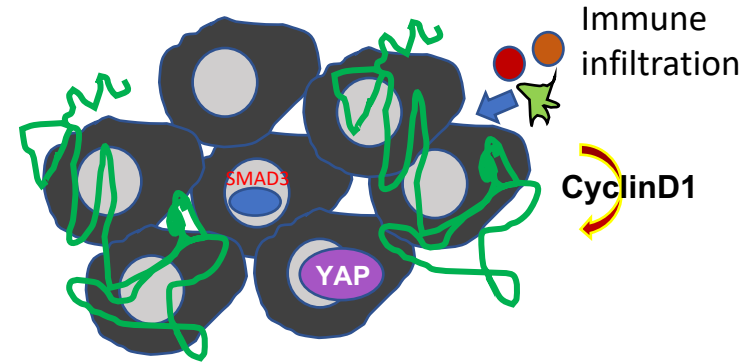
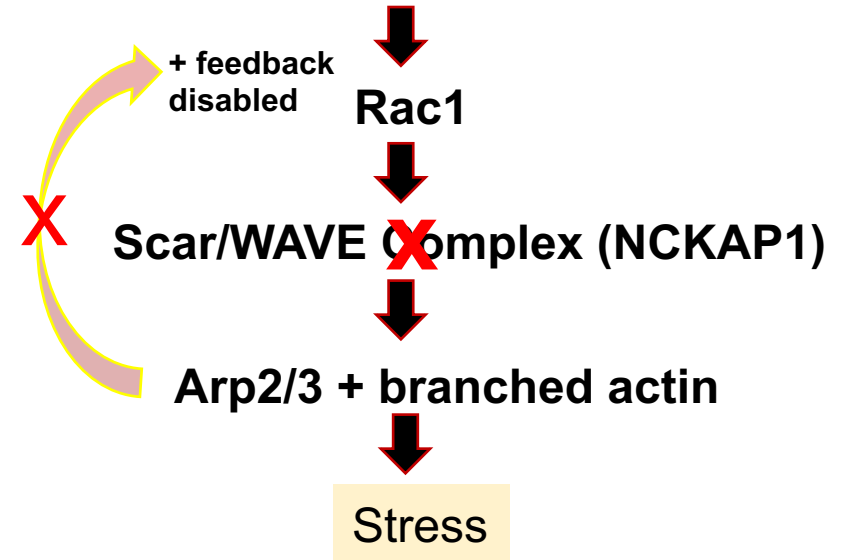




NCKAP1 +/+ melanoma

BRA^FV600E; PTEN loss

NCKAP1 -/- melanoma

BRA^FV600E; PTEN loss

TGF- β \rightarrow Nuclear SMAD3 \rightarrow Fibrosis \rightarrow Nuclear YAP \rightarrow Proliferation

Supplementary Information

The RAC1 target NCKAP1 plays a crucial role in progression of BRAF/PTEN -driven melanoma in mice

Supplementary Figure Legends

FIGURE S1. *Nckap1*^{fl/fl}; *Braf*^{V600E/+}; *Pten*^{wt/f} melanoma model schematics.

(a) *Nckap1* targeted allele. Screening oligos F = forward and R1, R2 = reverse, are shown as red arrows. (b) Schematics of the melanoma mouse model. (c) PCR showing the presence of FLP region in genomic DNA isolated from *Nckap1*^{wt/wt} and *Nckap1*^{fl/fl} endpoint tumors from n= 3 separate mice (wt – 294 bp; flp – 395 bp) or H₂O no DNA control. (d) PCR showing the efficiency of recombination in genomic DNA isolated from *Nckap1*^{wt/wt} and *Nckap1*^{fl/fl} endpoint tumors from n=2 separate mice (wt – 1200 bp; CRE-Del – 460 bp). (e) Kaplan-Meier tumor-free survival curve of mice with the indicated genotypes, *Nckap1*^{wt/wt} (n=15 mice), *Nckap1*^{fl/wt} (n=6 mice) and *Nckap1*^{fl/fl} (n=18 mice) under the genetic background of the *Tyr::CreER*^{T2+}; *Braf*^{V600E+}; *Pten*^{wt/f} following local administration of tamoxifen. Log-Rank (Mantel-Cox) test of survival plot revealed a significant difference (p<0.0001) between *Nckap1*^{wt/wt} and *Nckap1*^{fl/fl} genotypes. ****P<0.0001.

FIGURE S2. pERK staining upon *Nckap1* loss in melanoma.

(a-b) Representative images of pERK (p42/44) staining from *Nckap1*^{wt/wt} and *Nckap1*^{fl/fl} endpoint tumors under the genetic background *Tyr::CreER*^{T2+}; *Braf*^{V600E+}; *Pten*^{wt/f}. (c) Quantification of percentage of pERK positive nuclei/mm² from *Nckap1*^{wt/wt} (n=5) and

Nckap1^{ff} (n=6) tumors from separate mice. All error bars show mean \pm SEM. Unpaired t-test. ns = not significant. Scale bar is 100 μ m.

FIGURE S3. Increased TGF β signaling upon *Nckap1* loss

(a-d) Representative images of Picro Sirius Red (a-c) and S100 (b-d) staining from *Nckap1^{wt/wt}* and *Nckap1^{ff}* endpoint tumors with the genetic background *Tyr::CreER^{T2+}*; *Braf^{V600E+}*; *Pten^{wt/f}*. Scale bar is 1 mm. (e-f) Representative images of pSMAD3 staining from *Nckap1^{wt/wt}* and *Nckap1^{ff}* endpoint tumors under the genetic background *Tyr::CreER^{T2+}*; *Braf^{V600E+}*; *Pten^{wt/f}*. (g) Quantification of the percentage of pSMAD3 positive nuclei from *Nckap1^{wt/wt}* (n=5) and *Nckap1^{ff}* (n=6) tumors from separate mice. All error bars show mean \pm SD. Unpaired t-test. **P* < 0.05. Scale bar is 100 μ m.

FIGURE S4. p21 staining upon *Nckap1* loss in melanoma.

(a-b) Representative images of p21 staining from *Nckap1^{wt/wt}* and *Nckap1^{ff}* endpoint tumors with the genetic background *Tyr::CreER^{T2+}*; *Braf^{V600E+}*; *Pten^{wt/f}*. (c) Quantification of percentage of p21 positive nuclei/mm² from *Nckap1^{wt/wt}* (n=11) and *Nckap1^{ff}* (n=8) tumors from separate mice. All error bars show mean \pm SEM. Unpaired t-test. ns = not significant. Scale bar is 100 μ m.

FIGURE S5. YAP and pSRC staining upon *Nckap1* loss in melanoma.

(a) Representative images of YAP staining from *Nckap1^{wt/wt}* and (b) *Nckap1^{ff}* endpoint tumors with the genetic background *Tyr::CreER^{T2+}*; *Braf^{V600E+}*; *Pten^{wt/f}*. (c) Quantification of percentage of YAP positive cells/mm² from *Nckap1^{wt/wt}* (n=6) and *Nckap1^{ff}* (n=6) tumors from separate mice. (d) Representative images of pSRC (Tyr416) staining from *Nckap1^{wt/wt}* and (e) *Nckap1^{ff}* endpoint tumors. (f) Quantification of percentage of pSRC positive

cells/mm² from *Nckap1*^{wt/wt} (n=7) and *Nckap1*^{ff} (n=7) tumors from separate mice. All error bars show mean ± SEM. Unpaired t-test. *P<0.05, **P <0.01, ns = not significant. Scale bars are 100 μm.

FIGURE S6. Decreased activation of mTOR upon *Nckap1* loss in melanoma.

(a) Representative images of pS6 (Ser235/236) staining from *Nckap1*^{wt/wt} and (b) *Nckap1*^{ff} endpoint tumors with the genetic background *Tyr::CreER*^{T2+}; *Braf*^{V600E+}; *Pten*^{wt/f}. (c) Quantification of percentage of pS6 positive cells/mm² from *Nckap1*^{wt/wt} (n=8) and *Nckap1*^{ff} (n=8) tumors from separate mice. All error bars show mean ± SEM. Unpaired t-test. *P<0.05. Scale bar is 100 μm.

FIGURE S7. CD4 and CD3 staining upon *Nckap1* loss in melanoma.

(a) Representative images of anti-CD4 staining from *Nckap1*^{wt/wt} and (b) *Nckap1*^{ff} endpoint tumors under the genetic background *Tyr::CreER*^{T2+}; *Braf*^{V600E+}; *Pten*^{wt/f}. (c) Quantification of percentage of CD4+ positive T-cells/mm² from *Nckap1*^{wt/wt} (n=7) and *Nckap1*^{ff} (n=7) tumors. (d) Representative images of CD3+ T-cells staining from *Nckap1*^{wt/wt} and (e) *Nckap1*^{ff} endpoint tumors and (f) Quantification of percentage of CD3+ positive T-cells from *Nckap1*^{wt/wt} (n=7) and *Nckap1*^{ff} (n=7) tumors from separate mice. All error bars show mean ± SEM. Unpaired t-test. **P <0.01. Scale bar is 100 μM.

FIGURE S8. Cytokine array screen of *Nckap1* wt and knockout tumors.

(a) Representative images of cytokine blot prepared from *Nckap1*^{wt/wt} and (b) *Nckap1*^{ff} endpoint tumor lysates under the genetic background *Tyr::CreER*^{T2+}; *Braf*^{V600E+}; *Pten*^{wt/f}. (c) Quantification of relative signal intensity of various cytokines from *Nckap1*^{wt/wt} (n=2) and

Nckap1^{ff} (n=2) tumors using ImageJ. **(d)** Image of cytokine array template. See Table S3 for the key to the individual cytokines.

Figure S9. Model for how NCKAP1 loss affects BRAF^{V600E}; PTEN^{loss} melanoma. The left hand side shows melanomas in the BRAF^{V600E}; PTEN^{loss} model, where cyclinD1 activation mediates cell cycle progression downstream of oncogenic transformation. Rac1 is activated as a part of the oncogenic programme and triggers activation of the Scar/WAVE complex, leading to increased production of branched actin via Arp2/3 complex and enhanced motility. Feedback from branched actin sustains high activity of this pathway and promotes proliferation and invasion. The right-hand side shows a summary of some of our key findings in NCKAP1 null tumours, where the loop between rac1 and branched actin was broken by disabling the Scar/WAVE complex. Tumours displayed nuclear SMAD3 and higher levels of nuclear Yap, but the link with cell cycle progression and proliferation was broken by NCKAP1 loss, leading to fibrosis, inflammation and slowing of tumour growth. Immune infiltration was also enhanced, possibly due to increased TGF- β signalling. We thus propose that cytoskeletal dynamics downstream of oncogenic signalling represents an interesting target against tumour growth and progression for these melanomas.

Supplementary Methods

Transgenic mice generation and genotyping

The *Nckap1* flox mouse strain was created using a targeting vector (PG00182_Z_4_C05) obtained from the EuMMCR (European Mouse Mutant cell Repository) (www.eummcr.org) and generated by the IMPC/HMGU consortium for the The European Conditional Mouse Mutagenesis Program (EUComm). The targeting vector was linearised and transfected into

HM1 mESCs (Magin et al, 1992). Cells were selected with G418 (350 µg/ml) and surviving colonies were picked and screened for targeting by long range PCR (using the Roche Expand Long Template PCR System) from the lacZ/Neo-resistance cassette to sequences beyond the ends of the homology arms. Correct targeting of *Nckap1* was confirmed on DNA extracted from the ES cell clone by PCR on the 5' side

(CAGCAAGACCTGTCATAGATCTTATCCAAC and

CACAACGGGTTCTTCTGTTAGTCC; 6.5kb) and on the 3' side

(TCTATAGTCGCAGTAGGCGG

and CATGTTGTCCGCGTGACGGAGCAGC; 5.3kb). The presence of the isolated 3' loxP

site was also confirmed by PCR (GGGGTTAGAGAGTTGATCACATTG and

GAGACGTACCTGCCTCTGTCC; 398bp).

Following identification of correctly targeted clones, mouse lines were derived by injection of ES cells into C57BL/6J blastocysts according to standard protocols (Nagy et al. 2003).

After breeding of chimeras, germline offspring were identified by coat colour and the presence of the modified allele was confirmed with the 3' loxP primers described above.

Mice were subsequently crossed with a mouse line expressing Flpe

(Tg(ACTFLPe)9205Dym) to delete the selectable marker by recombination at the FRT sites

(Rodriguez et al. 2000). Correct removal of the lacZ gene and Neo cassette was confirmed by

PCR across the remaining FRT site (TGAGCTTTCACCTCCCTCACC and;

GCAACAACCTCCATCACTGG; 566bp).

Primers used for genotyping

The presence of floxed alleles was confirmed by PCR across the FRT site

(CTCTCTTGTCTACTGTGCAG and; CAAGAAACTTCGGTGTGATTT; 395bp) and the

efficiency of recombination was confirmed by PCR across the floxed site

(CTCTCTTGTCTACTGTGCAGG and; CTCGTAGACCAAAGCTAGCCTCAAG; 460bp).

See Figure S1a-d.

Generation of transgenic melanoma model

The *Nckap1* floxed mice are in C57BL/6J mixed background and show no phenotype in the absence of Cre. Tyrosinase Cre-ER^{T2} (*Tyr::Cre-ER^{T2}*) mice were previously described (Yajima et al, 2006). The *Braf* CA (*BrafV600E^{+/-}*) mice were described in (Dankort et al, 2007) and PTEN (*Pten^{fl/fl}*) floxed allele was described previously (Dankort et al, 2009). The *Nckap1* floxed mice were bred with animals under the genetic background *Tyr::Cre-ER^{+/-};BrafV600E^{+/-};Pten^{wt/fl}* to obtain *Tyr::Cre-ER^{+/-};BrafV600E^{+/-};Pten^{wt/fl}; Nckap1^{wt/wt}* (WT controls) *Tyr::Cre-ER^{+/-};BrafV600E^{+/-};Pten^{wt/fl};Nckap1^{fl/wt}* and *Tyr::Cre-ER^{+/-};BrafV600E^{+/-};Pten^{wt/fl};Nckap1^{fl/fl}* animals. Genotyping of the cohort was performed as described previously (Yajima et al., 2006, Dankort et al, 2007, Dankort et al, 2009) and by the company Transnetyx Inc (Memphis, TN, USA).

Transgene induction and animal monitoring

Mice were induced by application of 200 μ l of 2 mg/mL Tamoxifen (SIGMA – T5648) on the back skin of the animals after shaving. The induction regime was continued for five consecutive days. Animals were closely monitored for the formation of visible naevus (black spots) on the back skin and the date is logged. Tumors were measured three times a week and animals were sacrificed at endpoint (tumor size 1.2 cm diameter). Tumor volume was calculated by the formula: $V = W(2) \times L / 2$ where V is volume, W-width and L-Length of the tumor.

Cytokine analysis

Protein concentrations from tumor lysates were measured using Precision Red Advanced Protein Kit (Cytoskeleton, Inc). The Cytokine Array (Proteome Profiler Mouse XL Cytokine Array ARY028, R&D systems) was incubated overnight (4⁰C) with equivalent amount of protein lysates from different genotypes and the membrane was processed according to manufacturer's instructions. The pixel intensity of the Cytokine spots was calculated according to the manufacturer's instructions using Image J and relative intensity values were plotted using Prism 8 (GraphPad software).

Immunohistochemistry

Formalin-fixed paraffin-embedded (FFPE) sections were processed by standard histology processing techniques as previously described (Li et al., 2012b). The following antibodies were used: BrdU (BD biosciences 347580, pH6 1:200), CD3 (AbCam ab16669, pH6 1:50), CD4 (eBioscience 14-9766-82, ER2 Leica, 1:500), CD8 (eBioscience 14-0808-82, ER2 Leica, 1:500), S100A9 (Santa Cruz sc-8115, pH6 1:1000), pSMAD3 (Abcam ab52903, pH6, 1:40), aSMA (Sigma-Aldrich A2547, pH6, 1:25000), CD31 (Abcam ab28364, pH6, 1:75), ki67 (Abcam ab16667, pH6, 1:100), F4-80 (Abcam ab6640, Enz 1 Leica, 1:100), pERK1/2 (Cell Signalling 9101, pH6, 1:400), HIF1a (BD biosciences 610959, pH6, 1:50), YAP (Cell Signalling 4912, pH6, 1:50), and cyclinD1 (Abcam ab134175, pH6, 1:200). All primary antibody incubations were performed for 40 minutes except for cyclinD1 which is for 2hrs. Picro Sirius Red staining was used to stain for collagen and fibrin in the tissues. Briefly, sections were rehydrated and immersed for 2hrs in Picro Sirius Red solution (0.1% Direct red 80 (Sigma, 41496LH) and 0.1% Fast green FCF, Raymond Lamb, S142-2). To stain for mast

cells, toluidine blue staining was used. Briefly, rehydrated sections were immersed for 5 minutes in toluidine blue solution (0.1% toluidine blue in 1% NaCl solution). Slides were dehydrated using standard protocols post staining and mounted for analysis. Images were taken using Olympus BX51 microscope and/or slides were scanned using Leica SCN 400f scanner. The scanned images were processed and analysed using HALO Image Analysis Software (Indica Labs).

Journal Pre-proof